CAMPAIGN CRUISE REPORT · PACIFIC COLOR 2025

FECOP
FEDERACIÓN COSTARRICENSE DE PESCA

Pacific Color 2025

Gulf of Nicoya, Central Pacific Shelf,
and Golfo Dulce, Costa Rica

CAMPAIGN CRUISE REPORT

February 2025

PACIFIC COLOR
2025

FECOP
FEDERACION COSTARRICENSE DE PESCA
NASA
UNA
UNIVERSIDAD
NACIONAL
COSTA RICA
UNIVERSIDAD DE
COSTA RICA

CAMPAIGN CRUISE REPORT

Pacific Color 2025

Gulf of Nicoya, Central Pacific Shelf,
and Golfo Dulce, Costa Rica

Date	August 2026
Document Type	Campaign Cruise Report
Correspondence	mmarrari@fecop.org
Data DOI	10.5067/SeaBASS/PCOLOR2025/DATA001
Vessel	M/V *Amejaye* (64-ft Viking sportfishing yacht)
Cruise Dates	February 17–21, 2025
Study Area	Costa Rican Pacific Coast — Gulf of Nicoya, offshore waters, Golfo Dulce, and coastal transects (23 stations total)
Keywords	ocean color; phytoplankton; PACE; HPLC; harmful algal blooms; Costa Rica; Gulf of Nicoya; Golfo Dulce; bio-optics; Eastern Tropical Pacific; remote sensing; DALEC; AVIRIS-3

Suggested Citation

Marrari, M., Aurin, D., Chapman, J., Chaves, J. E., Chaves-Campos, J., Freeman, S., García Rojas, A., Luis, K., Mannino, A., Marín, C., Martinez, D., Mug, M., Podest, E., Schimel, D., Toro Farmer, G., Vargas, L., Vargas, M., & Vega, L. (2026). *Pacific Color 2025: Campaign Cruise Report.* Federación Costarricense de Pesca / NASA. 10.5067/SeaBASS/PCOLOR2025/DATA001

BibTeX:

```
@techreport{PacificColor2025,
  author = {Marrari, Marina and Aurin, Dirk and Chapman, John and Chaves, Joaquín E. and Chaves-Campos, Johel and Freeman,
            Scott and García Rojas, Andrea and Luis, Kelly and Mannino, Antonio and Marín, Carolina and Martinez, Damián
            and Mug, Moisés and Podest, Erika and Schimel, David and Toro Farmer, Gerardo and Vargas, Lucía and Vargas,
            Maribelle and Vega, Luis},
  title = {Pacific Color 2025:  Campaign Cruise Report},
  institution = {Federación Costarricense de Pesca/ NASA},
  year = {2026},
  doi = {10.5067/SeaBASS/PCOLOR2025/DATA001}
}
```

Data status: *Preliminary — data have not yet undergone full quality control. Values are subject to change. Version 1.0.*

Contents

Campaign Participants and Contributors **3**

1 Introduction **4**
1.1 Background and Mission Context . . . 4
1.2 Campaign Objectives . . . 4
1.3 Collaborative Framework . . . 5
1.4 Regional Significance . . . 5
1.5 Campaign Overview . . . 6
1.6 Report Objectives and Dissemination . . . 6

2 Study Area Description **7**
2.1 Geographic Setting and Oceanographic Context . . . 7
2.2 Gulf of Nicoya: Central America's Premier Estuarine System . . . 8
2.3 Golfo Dulce: A Tropical Fjord Ecosystem . . . 8
2.4 The Southern Pacific Shelf: Sierpe-Terraba Delta, Coronado Bay, and Adjacent Waters . 9
2.5 Ecological Significance and Marine Biodiversity . . . 9
2.6 Sport Fishing Tourism: Economic Engine and Conservation Driver . . . 10
2.7 Artisanal Fisheries and Coastal Communities . . . 10
2.8 Conservation and Marine Protected Areas . . . 10

3 Methods **10**
3.1 Campaign Design and Multiplatform Observation Strategy . . . 10
3.2 Cruise Track and Station Plan . . . 11
3.2.1 Cruise Legs and Timing . . . 11
3.3 Above-Water Radiometry: DALEC System . . . 11
3.3.1 System Description and Theoretical Background . . . 11
3.3.2 DALEC Instrumentation . . . 11
3.3.3 Deployment Configuration . . . 13
3.3.4 Operational Protocols . . . 13
3.3.5 Remote Sensing Reflectance Derivation . . . 14
3.3.6 Data Processing and Quality Control . . . 14
3.3.7 Data Archiving . . . 14
3.4 PACE Satellite Observations . . . 14
3.4.1 PACE Mission Overview and Ocean Color Instrument . . . 14
3.4.2 PACE Validation Objectives for Pacific Color . . . 14
3.4.3 PACE Overpass Coordination and Matchup Criteria . . . 14
3.4.4 PACE Data Products and Processing . . . 15
3.4.5 Validation Analysis Approach . . . 15
3.4.6 Regional Algorithm Development . . . 15
3.4.7 Airborne Hyperspectral Imagery (AVUELO / AVIRIS-3) . . . 15
3.5 Water Sample Collection . . . 15
3.5.1 Phytoplankton Pigments Analyzed by HPLC . . . 15

3.6 Phytoplankton Sampling and Identification . . . 17
3.6.1 Net Tow Sampling . . . 17
3.6.2 Niskin Bottle Water Samples . . . 17
3.6.3 Field Observations and Live Microscopy . . . 17
3.6.4 Sample Processing and Laboratory Analysis . . . 17
3.6.5 Data Products and Timeline . . . 19
3.7 Oceanographic Measurements . . . 19
3.7.1 CTD Profiling . . . 19
3.7.2 Water Transparency . . . 19
3.8 Zooplankton and Fish Larvae Sampling . . . 19

4 Preliminary Results **19**
4.1 General Oceanographic Observations . . . 19
4.1.1 Surface Hydrography . . . 19
4.1.2 Surface Nutrient Distributions . . . 20
4.2 Additional Water Measurements . . . 21
4.3 Phytoplankton Pigment Distributions . . . 22
4.3.1 Gulf of Nicoya . . . 22
4.3.2 Offshore Stations . . . 22
4.3.3 Coastal Stations . . . 23
4.3.4 Golfo Dulce . . . 23
4.3.5 Coastal Return Transect . . . 23
4.4 Phytoplankton Abundance . . . 23
4.4.1 Taxonomic Composition . . . 23
4.4.2 Qualitative Abundance Distribution (Days 1–3, Stations 1–14) . . . 26
4.4.3 Cyanobacteria . . . 27
4.4.4 Cell Abundance and Taxonomic Composition — Preliminary Results . . . 28
4.5 Fish Larvae and Ichthyoplankton . . . 29
4.5.1 Larval Fish Diversity and Taxonomic Composition . . . 29
4.5.2 Collection Status and Future Work . . . 31
4.5.3 PACE Satellite Data Acquisition and Spatial Coverage . . . 31
4.5.4 Preliminary DALEC and PACE Radiometry Matchups . . . 31
4.5.5 Spatial Distribution of Satellite Retrievals and Environmental Constraints . . . 35
4.5.6 Level-3 Chlorophyll *a* Composites and HPLC Matchups . . . 35
4.5.7 AVUELO / AVIRIS-3 Airborne Observations . . . 36

A Appendix **43**
A.1 Data Management Notes . . . 43
A.1.1 Data Repositories and Formatting . . . 43
A.1.2 Discoverability and DOI . . . 43
A.1.3 Data Usage, Embargo, and Citation . . . 43
A.2 HPLC Replicate Statistics . . . 44
A.2.1 Analytical Precision . . . 44

Campaign Participants and Contributors

Table 1. Pacific Color 2025 campaign participants and contributors.

Institution	Participants
FECOP	Marina Marrari (Chief Scientist) Moisés Mug Damián Martinez Johel Chaves-Campos Lucía Vargas
NASA GSFC	Joaquín E. Chaves (co-Chief Scientist) Scott Freeman Antonio Mannino Gerardo Toro Farmer Dirk Aurin
NASA JPL	Kelly Luis David Schimel Erika Podest John Chapman
UCR	Maribelle Vargas
UNA	Andrea García Rojas Carolina Marín Luis Vega

1. Introduction

1.1 Background and Mission Context

The Pacific Color (PCOLOR) campaign represents a critical collaboration between the Costa Rican Fishing Federation (FECOP), NASA's Plankton, Aerosol, Cloud, ocean Ecosystem (PACE) mission, and Costa Rican academic researchers from the University of Costa Rica (UCR) and the National University of Costa Rica (UNA), with additional support from the University of South Florida (USF), to advance our understanding of marine ecosystem dynamics along the Pacific coast of Costa Rica. This field validation effort was conducted in collaboration with the broader Airborne Validation: Unified Experiment Land to Ocean (AVUELO) project, which seeks to calibrate a new class of spaceborne hyperspectral imagers for tropical vegetation and ocean research.

The AVUELO project, led by NASA and the Smithsonian Tropical Research Institute (STRI) in February 2025, deployed the Airborne Visible-Infrared Imaging Spectrometer 3 (AVIRIS-3) to collect hyperspectral imagery across terrestrial and marine sites in Panama and Costa Rica. While AVUELO's terrestrial components focused on forest canopy characterization and volcanic landscapes, the marine component, conducted in collaboration with the PACE team, concentrated on Costa Rica's Pacific coastal waters.

The five-day Pacific Color expedition (February 17–21, 2025) brought together twelve scientists from four institutions aboard the sportfishing vessel *Amejaye*. This research cruise represents the first of several sampling exercises planned over an 18-month period within FECOP's PACE Early Adopter Project, designed to build sustained observation capacity and develop operational satellite-based monitoring tools for Costa Rican waters.

Following the launch of the PACE satellite in 2024, this integrated airborne and shipboard validation effort provides essential ground-truth data to support the development and refinement of satellite-derived ocean color products for tropical and subtropical coastal waters. The combination of spaceborne PACE observations (∼220 wavelengths from the Ocean Color Instrument), airborne AVIRIS-3 hyperspectral imagery, and comprehensive *in situ* measurements creates a multi-scale validation framework that addresses the unique challenges of coastal ocean remote sensing in optically complex tropical waters.

PACE's hyperspectral Ocean Color Instrument (OCI) offers unprecedented capability to detect and characterize phytoplankton community composition from space. However, the translation of satellite-observed spectral signatures into meaningful biological and biogeochemical information requires comprehensive *in situ* validation datasets. The Pacific Color initiative addresses this need while simultaneously building regional capacity for sustained ocean observation and marine resource management.

1.2 Campaign Objectives

The Pacific Color campaign was designed to achieve four primary objectives:

1. **Characterize the optical conditions of coastal waters** along Costa Rica's Pacific coast, including apparent optical properties (remote sensing reflectance) and inherent optical properties (absorption and scattering by phytoplankton, chromophoric dissolved organic matter, and suspended particles).

2. **Assess phytoplankton community composition** and determine dominant species and their pigment signatures, through integration of microscopic identification, HPLC pigment analysis, and flow cytometric enumeration of prokaryotic phytoplankton.

3. **Develop novel satellite tools to identify and monitor harmful algal blooms (HABs)** from space in near real-time, linking field observations of phytoplankton community composition with optical signatures detectable by PACE's hyperspectral capabilities.

4. **Support validation and calibration of NASA's PACE hyperspectral ocean color mission**, providing essential ground-truth measurements for assessing product accuracy, refining atmospheric correction algorithms, and evaluating phytoplankton community composition retrieval algorithms.

These objectives converge on the overarching goal of developing operational satellite products to detect, identify, and monitor red tides and other algal blooms, ultimately establishing an early alert system distributed through FECOP's mobile application PezCA.

1.3 Collaborative Framework

The Pacific Color project exemplifies multi-institutional collaboration integrating international space-based and airborne observation capabilities with local expertise in tropical marine ecosystems.

The expedition was led, coordinated, and partially funded by FECOP, with additional financial support from NASA covering vessel fuel, equipment loans (including the DALEC hyperspectral radiometer), HPLC and CDOM analytical costs, travel expenses for three NASA researchers, and technical training. The University of South Florida (USF) contributed filtration and oceanographic equipment along with training in sampling protocols. UNA covered equipment and travel expenses for three researchers, while UCR supported equipment, laboratory analyses, and supplies for one researcher. NASA JPL contributed AVUELO airborne campaign costs and hyperspectral data collection and analysis.

Logistical support was generously provided by Crocodile Bay Resort and Botanika, which donated accommodations in the Golfo Dulce region. Marina Pez Vela and Safe Harbor Los Sueños Marina assisted with vessel docking and provided facilities for equipment preparation and sample processing.

The partnership reflects a commitment to open science and capacity building, emphasizing:

- **Multi-scale validation of satellite and airborne remote sensing algorithms** for tropical coastal waters
- **Harmful algal bloom (HAB) detection and forecasting** to protect public health and marine resources
- **Sustainable fisheries management** through improved understanding of phytoplankton dynamics
- **Support for the blue economy** through actionable information for fishing communities and coastal managers
- **Regional capacity building** through technology transfer, training, and collaborative research with Costa Rican institutions
- **Public engagement through accessible information** products distributed via the PezCA mobile application

1.4 Regional Significance

Costa Rica's Pacific coast encompasses diverse oceanographic environments, from the productive inner waters of the Gulf of Nicoya, Central America's largest estuarine system, to the unique tropical fjord ecosystem of Golfo Dulce (Vargas, 1995, 2016; Svendsen et al., 2006). These coastal waters are influenced by large-scale oceanographic features that drive productivity and ecosystem dynamics across the Central American Pacific shelf (Fiedler and Talley, 2006; Kessler, 2006).

The Costa Rica Dome, a seasonally persistent thermocline shoaling feature located approximately 500–700 km offshore, enriches surface waters during the boreal winter and spring (February–April) when forced by the Papagayo wind jet (Fiedler, 2002; Wyrtki, 1964; Fiedler et al., 2017). The Papagayo Jet drives coastal upwelling in the northern Pacific region during the boreal winter dry season (December–April), fueling phytoplankton blooms (Amador et al., 2006; Brenes et al., 2003; Fiedler,

2002). The Costa Rica Coastal Current (CRCC), flowing northwestward along the coast, connects these productivity hotspots and transports water masses, nutrients, and plankton communities along the shelf (Brenes, 1985; Brenes et al., 2008; Kessler, 2006).

Understanding the "boom-bust" cycles of phytoplankton productivity in these waters is essential for:

- **Predicting fisheries productivity** and supporting sustainable harvest strategies
- **Early detection of harmful algal blooms** (red tides) that can cause fish kills, shellfish toxicity, and economic disruption
- **Monitoring long-term environmental changes** related to climate variability, coastal development, and anthropogenic nutrient inputs
- **Supporting marine protected area management** and ecosystem-based conservation planning

1.5 Campaign Overview

The February 2025 Pacific Color expedition departed from Marina Los Sueños in Herradura Bay on the central Pacific coast and proceeded southward to Golfo Dulce over five days (February 17–21, 2025), covering approximately 250 km of coastline (Fig 1.1). The campaign was conducted aboard the sportfishing vessel *Amejaye*, capitalizing on the operational capabilities and local knowledge of the Costa Rican fishing community. Operations were coordinated temporally with AVUELO airborne hyperspectral overflights.

The field program sampled 23 stations spanning the gradient from estuarine conditions in the Gulf of Nicoya through coastal waters to the deep tropical fjord of Golfo Dulce. The multiplatform observation strategy integrated:

- **Satellite observations from NASA's PACE mission**, with daily overpasses at approximately 1300 local time collecting hyperspectral data at ∼220 wavelengths
- **Airborne hyperspectral imagery** from NASA JPL's AVIRIS-3 high-resolution spectrometer
- **Continuous shipboard optical measurements** from the bow-mounted DALEC hyperspectral radiometer collecting data at 220 wavelengths during transit and at stations
- **Comprehensive *in situ* sampling** at each station for phytoplankton community characterization, optical properties, and oceanographic conditions

At each of the 23 stations, the team collected:

- **Surface water samples for HPLC pigment analysis**, chlorophyll *a* concentration, CDOM, nutrients, heavy metals, microplastics, and bacteria
- **Phytoplankton samples** using 20-µm nets for species identification and 1.7-liter Niskin bottles for cell counts
- **Oceanographic profiles** using handheld CTD (temperature, salinity, pH)
- **Water transparency measurements** with Secchi disk
- **Zooplankton and fish larvae** samples using 500-µm nets (on a subset of stations)

1.6 Report Objectives and Dissemination

This cruise report documents the methods, preliminary findings, and data products from the February 2025 Pacific Color field effort and the relevant AVUELO campaign marine component activities off the coast of Costa Rica. The report is designed to serve multiple audiences:

- **Research scientists** engaged in ocean color remote sensing, phytoplankton ecology, and coastal oceanography

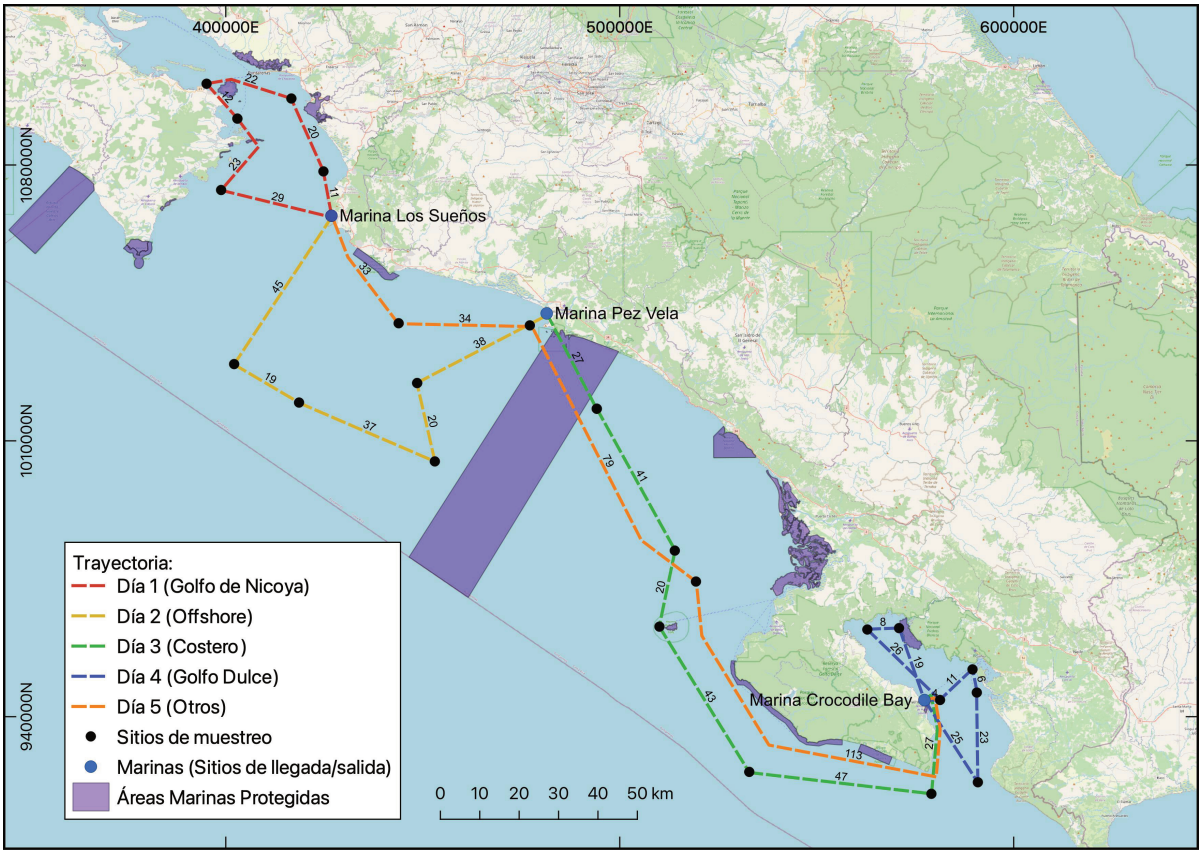


Figure 1.1. Pacific Color campaign study area. The five-day expedition (February 17–21, 2025) covered approximately 500 km along Costa Rica's Pacific coast from Herradura to Golfo Dulce aboard the M/V *Amejaye*. Black circles indicate the sampling stations. Purple polygons denote marine protected areas.

- **Marine resource managers** responsible for fisheries regulation and marine protected area oversight
- **Public health officials** concerned with HAB monitoring and early warning
- **NGO partners and community stakeholders** involved in marine conservation and sustainable blue economy initiatives
- **Fishing communities and tourism operators** who will benefit from satellite-derived information products
- **Funding agencies and program managers** evaluating Pacific Color and AVUELO outcomes

The report provides essential metadata and quality documentation to support data archiving in NASA's SeaBASS (SeaWiFS Bio-optical Archive and Storage System) repository, ensuring long-term accessibility of these field validation measurements for the international ocean color community.

2. Study Area Description

2.1 Geographic Setting and Oceanographic Context

The Pacific Color campaign covered approximately 250 km of Costa Rica's Pacific coastline, spanning from the inner Gulf of Nicoya (approximately 10°N, 85°W) southward to Golfo Dulce (approximately 8.5°N, 83.5°W). This region represents one of the most oceanographically diverse and ecologically productive sections of the Central American Pacific

coast, encompassing estuarine, embayment, and open coastal waters that support critical fisheries and marine-dependent economies (Cortés, 2016; Fiedler and Lavín, 2016).

At the regional scale, the Costa Rica Dome (see Section 1.4) serves as a major source of nutrient enrichment to surface waters (Broenkow, 1964; Fiedler, 2002; Wyrtki, 1964). This cyclonic feature exhibits a four-stage annual cycle, with strongest thermocline shoaling and biological productivity during February–April when forced by the Papagayo wind jet, followed by westward expansion during July–November (Fiedler, 2002; Fiedler et al., 2017). The Costa Rica Coastal Current (CRCC) flows northwestward along the shelf during much of the year, creating alongshore gradients in water mass properties, nutrient concentrations, and biological communities (Brenes, 1985; Brenes et al., 2008; Kessler, 2006).

2.2 Gulf of Nicoya: Central America's Premier Estuarine System

The Gulf of Nicoya is the largest estuarine system in Central America, extending approximately 80 km inland with a surface area exceeding 1,500 km^2 (Vargas, 1995, 2016). The gulf exhibits classical estuarine circulation, with freshwater input from the Tempisque and Tárcoles river systems creating strong horizontal and vertical gradients in salinity, temperature, and nutrient concentrations (Epifanio et al., 1983; Kress et al., 2002; Palter et al., 2007).

The Tárcoles River drains Costa Rica's densely populated Central Valley, including San José and important agricultural areas, delivering approximately 60% of total riverine nitrogen and 27% of phosphorus inputs to the gulf (Chaves, 1997). Only about one-third of the Tárcoles nitrogen export derives from human sewage, with the remainder attributed to livestock farming, crop production, and other agricultural activities. This anthropogenic nutrient loading has raised concerns about eutrophication, though large oceanic nutrient contributions (approximately 85% of nitrogen and 75% of phosphorus from coastal ocean sources) may buffer against some impacts (Chaves, 1997). This assessment is nearly three decades old; given the substantial growth of Costa Rica's Central Valley population and the lack of tertiary wastewater treatment, the proportion attributable to urban sewage may be considerably higher today.

The Gulf of Nicoya has been intensively studied over the past several decades, providing a valuable baseline for understanding long-term trends in water quality, HABs, and ecosystem responses to climate variability and coastal development (Vargas, 1995, 2016; Gocke et al., 1990; Brugnoli-Olivera and Morales-Ramírez, 2008). The optical complexity of these waters, characterized by high concentrations of suspended sediments, CDOM, and variable phytoplankton communities, poses significant challenges for satellite remote sensing, making *in situ* validation datasets essential (Hargraves and Víquez M., 1985; Kress et al., 2002).

2.3 Golfo Dulce: A Tropical Fjord Ecosystem

Golfo Dulce, located in the southern Pacific region near the border with Panama, represents a unique tropical fjord environment, one of only a handful of such systems worldwide (Svendsen et al., 2006). The embayment extends approximately 50 km inland, with a maximum depth exceeding 200 m in the inner basin separated from a shallow outer basin by a sill at approximately 60 m depth (Svendsen et al., 2006). Unlike the Gulf of Nicoya, Golfo Dulce is characterized by limited freshwater input from four rivers, steep bathymetry, and restricted deep-water circulation creating persistent anoxic conditions (Svendsen et al., 2006; Quesada-Alpízar and Morales-Ramírez, 2004; Dalsgaard et al., 2003).

The gulf exhibits strong year-round stratification with an upper brackish layer of 40–50 m overlying a nearly homogeneous high-salinity layer below (Svendsen et al., 2006). The upper water column supports primary productivity fueled by riverine nutrient inputs, nutrient regeneration from the anoxic deep basin, and exchange with coastal waters at the entrance (Quesada-Alpízar and Morales-Ramírez,

2004). The surrounding landscape, largely covered by intact tropical rainforest within the Osa Peninsula conservation corridor, results in terrigenous inputs dominated by organic material from pristine sources rather than high sediment loads (Hebbeln and Cortés, 2001; Morales-Ramírez, 2011).

2.4 The Southern Pacific Shelf: Sierpe-Terraba Delta, Coronado Bay, and Adjacent Waters

The coastal and offshore waters between the Gulf of Nicoya and Golfo Dulce encompass one of the least hydrographically characterized regions of the Costa Rican Pacific, despite its considerable ecological and economic importance. This stretch of coastline includes several features of outstanding biological significance: the Sierpe-Terraba deltaic system, Costa Rica's largest river delta and wetland complex; Coronado Bay, the broad embayment immediately offshore of the delta; Isla del Caño, home to some of the most productive Pacific coral reefs in Central America; and Parque Marino Ballena, a marine protected area near Uvita that encompasses coral reefs, rocky outcrops, and important cetacean habitat (Cortés, 2016). The region also supports active commercial and sport fisheries, attracting considerable fishing effort from both national and international fleets throughout the year.

The Sierpe-Terraba system is fed by the Río Térraba and Río Sierpe, which together drain the largest drainage watershed in Costa Rica and discharge into a complex deltaic network bordered by Costa Rica's most extensive mangrove forests (Acuña Piedra and Quesada-Román, 2017). Despite the ecological prominence of these mangroves, which have been the subject of several biological and conservation studies, the hydrographic and oceanographic characteristics of the adjacent coastal and offshore waters remain poorly documented. The earliest systematic hydrographic observations in this region were conducted during the 1993–1994 *Victor Hensen* expedition, which provided the first reported measurements of water column properties in Coronado Bay and the adjacent shelf (Wolff and Vargas, 1994). That survey found no detectable influence of the Sierpe and Terraba rivers on the offshore hydrographic properties of Coronado Bay, with nutrient vertical distributions indistinguishable from those of the contiguous Eastern Tropical Pacific oceanic waters. No differences in hydrographic conditions were observed between the December 1993 and February 1994 cruise legs, suggesting relatively stable oceanographic conditions during the dry season. To our knowledge, no systematic hydrographic or bio-optical surveys have been conducted in this region since that expedition, representing a gap of over three decades in the observational record.

More recently, Lizano (2015) examined the oceanographic dynamics immediately offshore of the Térraba-Sierpe National Wetland in the context of ongoing mangrove die-off, reporting that sea level rise driven by coastal subsidence, has altered wave dynamics, beach profiles, and sediment transport patterns in the area. The offshore (**Stn. 6**–**Stn. 9**) and coastal return (**Stn. 21**–**Stn. 23**) transects of the Pacific Color 2025 campaign traversed this poorly characterized region, providing what are likely the first surface bio-optical, and pigment measurements collected here, and establishing a valuable baseline for future monitoring and remote sensing validation in this ecologically and economically significant area.

2.5 Ecological Significance and Marine Biodiversity

The oceanographic diversity of Costa Rica's Pacific coast creates a productivity gradient supporting exceptional marine biodiversity (Cortés, 2016; Fiedler and Lavín, 2016). Phytoplankton communities range from coastal diatom-dominated assemblages during upwelling events to mixed communities including dinoflagellates, coccolithophores, and cyanobacteria in stratified offshore waters (Hargraves and Víquez M., 1985; Brugnoli-Olivera and Morales-Ramírez, 2008).

The region also experiences periodic harmful algal blooms (HABs), known locally as "red tides"

(*marea roja*), which can cause mass mortality events affecting fish, sea turtles, dolphins, and seabirds (Brugnoli-Olivera and Morales-Ramírez, 2008; Gocke et al., 1990). Early detection and monitoring of HABs is a critical management priority that can be significantly enhanced through satellite remote sensing validated with field observations.

2.6 Sport Fishing Tourism: Economic Engine and Conservation Driver

Sportfising tourism represents one of the most significant components of Costa Rica's Pacific coastal economy. The waters from the Nicoya Peninsula to Golfo Dulce are internationally recognized as world-class billfish destinations, attracting recreational anglers from North America, Europe, and beyond (Fiedler et al., 2017).

Costa Rica's sportfising industry spans several key regions: Guanacaste Province in the north, Safe Harbor Los Sueños Marina in Herradura near the mouth of the Gulf of Nicoya, Quepos with Marina Pez Vela in the central Pacific, and southern destinations including Golfito, Puerto Jiménez, and Drake Bay. The Pacific Color campaign directly supports sportfising sustainability by advancing our ability to monitor oceanographic conditions that drive fish distribution and abundance, and by providing early warning capabilities for harmful algal blooms.

2.7 Artisanal Fisheries and Coastal Communities

Artisanal fisheries remain the primary livelihood for many coastal communities throughout the region. Small-scale fishers operating from open boats (*pangas*) target diverse species including snappers, groupers, jacks, corvinas, and small pelagics for domestic markets and local consumption. The Gulf of Nicoya hosts particularly important artisanal shrimp and finfish fisheries (Vargas, 2016).

2.8 Conservation and Marine Protected Areas

The study region includes several marine protected areas (MPAs; Fig 1.1) and biological corridors designed to conserve marine biodiversity while supporting sustainable use. The Osa Peninsula, bordered by Golfo Dulce, forms part of Costa Rica's most extensive remaining lowland tropical rainforest and includes critical marine habitats within Corcovado National Park and associated reserves (Morales-Ramírez, 2011). Satellite remote sensing, when properly validated and calibrated, offers a cost-effective tool for MPA monitoring, assessment of management effectiveness, and detection of environmental changes (Lizano et al., 2001).

3. Methods

3.1 Campaign Design and Multiplatform Observation Strategy

The Pacific Color campaign employed a coordinated multiplatform observation strategy providing comprehensive characterization of bio-optical properties across multiple spatial scales, from satellite (∼1 km) through airborne (∼4 m) to shipboard (<1 m) resolution, through four complementary observation components:

- **PACE/OCI:** Hyperspectral data at ∼220 wavelengths during daily overpasses at ∼1300 local time, ∼1 km spatial resolution
- **AVIRIS-3:** Airborne hyperspectral imagery at ∼4 m pixels, coordinated temporally and spatially with vessel operations
- **DALEC:** Bow-mounted hyperspectral radiometer collecting above-water remote sensing reflectance continuously at 220 wavelengths
- **In situ discrete sampling:** Biological, chemical, and optical characterization at 23 stations

3.2 Cruise Track and Station Plan

The five-day expedition (February 17–21, 2025; Fig 1.1, Table 3.1) departed from Herradura/Marina Los Sueños on the central Pacific coast and proceeded southward to Golfo Dulce before returning north along a coastal route, covering approximately 500 km total distance.

3.2.1 Cruise Legs and Timing

Day 1 (February 17, 2025): Gulf of Nicoya Transect. Departure from Herradura/Safe Harbor Los Sueños Marina, transit into Gulf of Nicoya. Five stations (**Stn. 1**–**Stn. 5**) spanning the estuarine gradient from the outer gulf (Tárcoles River influence) through mid-gulf (Caldera, San Lucas, Paquera) to the inner gulf (Tambor). Direct overlap with AVIRIS-3 overflight covering the Gulf of Nicoya. Sampling period: 1350–1855 GMT. Overnight: Herradura.

Day 2 (February 18, 2025): Central Pacific Offshore Transect. Departure from Herradura/ Safe Harbor Los Sueños Marina, offshore transect southward. Four offshore stations (**Stn. 6**–**Stn. 9**) in productive coastal waters west of the continental shelf. Sampling period: 1417–1957 GMT. Overnight at Quepos, Marina Pez Vela.

Day 3 (February 19, 2025): Southern Pacific and Golfo Dulce Approach. Extended transit from Quepos to Golfo Dulce entrance. Six coastal stations (**Stn. 10**–**Stn. 15**) along the southern Pacific coast including Savegre, Sierpe (river plume), Bajo del Diablo, and approaching Golfo Dulce entrance. Sampling period: 1256–2128 GMT. Overnight anchorage in inner gulf.

Day 4 (February 20, 2025): Golfo Dulce Survey. Five stations (**Stn. 16**–**Stn. 20**) within Golfo Dulce from entrance (Boca Golfo) through inner basin (Coto, Cocodrilo, Golfito, Rincón, Esquinas). Sampling period: 1346–1800 GMT. Overnight: inner Golfo Dulce anchorage.

Day 5 (February 21, 2025): Coastal Return Transect. Return transit northward along coastal route. Three nearshore coastal stations (**Stn. 21**–**Stn. 23**): Sierpe coastal, Quepos coastal, Parrita coastal. Sampling period: 1435–1806 GMT. Return to Herradura/Marina Los Sueños.

3.3 Above-Water Radiometry: DALEC System

3.3.1 System Description and Theoretical Background

Continuous above-water radiometric measurements were acquired using the Dynamic Above-water Radiance and Irradiance Collector (DALEC; Fig 3.1), an autonomous hyperspectral radiometer system developed by In Situ Marine Optics (IMO, Australia) and provided on loan by NASA. The DALEC is specifically designed for underway measurements from moving vessels, integrating three independent radiometric channels with motion sensors and motorized azimuth control to maintain optimal viewing geometry relative to sun position (Brando et al., 2016).

In above-water radiometry, the measurement geometry is defined by the solar zenith angle (θ_z), the sea-viewing zenith angle (θ_v), the sky-viewing zenith angle (θ_s), and the relative azimuth angle (φ) away from the solar plane. Measurements of the total upwelling sea surface radiance $L_u(\theta_v, \varphi, \lambda)$ consist of the water-leaving radiance just above the sea surface $L_w(\theta_v, \varphi, \lambda)$ as well as the surface-reflected radiance $L_{sr}(\theta_v, \varphi, \lambda)$. The sea surface radiance reflection coefficient $\rho(\theta_v, \varphi, \theta_z, \lambda)$ can be used to estimate L_{sr} from sky radiance measurements: $L_{sr} = \rho L_{sky}$.

3.3.2 DALEC Instrumentation

The DALEC sensor head contains three compact Carl Zeiss Monolithic Miniature Spectrometers (MMS1, UV-VIS-NIR enhanced), along with integrated GPS and inertial motion sensors (pitch and roll). Each spectroradiometer records approximately 200 channels covering 310–1150 nm, with spectral resolution of 10 nm and spectral sampling at ∼3.3 nm intervals. The system is calibrated

Table 3.1. Pacific Color 2025 campaign station positions and characteristics. Station locations span from the outer Gulf of Nicoya (9.95°N) to the inner Golfo Dulce (8.32°N), covering approximately 1.7° of latitude. Local names reference nearby geographic features or communities.

Stn.	Name	Transect	Date	Time (GMT)	Lat (°N)	Lon (°W)	Regional Context
1	Tárcoles	Golfo de Nicoya	2/17/25	13:50	9.7518	84.6857	Outer gulf, Tárcoles River plume
2	Caldera	Golfo de Nicoya	2/17/25	15:08	9.9189	84.7603	Mid-gulf, port of Caldera proximity
3	San Lucas	Golfo de Nicoya	2/17/25	16:35	9.9523	84.9566	Mid-gulf, San Lucas Island region
4	Paquera	Golfo de Nicoya	2/17/25	17:39	9.8725	84.8851	Mid-gulf, eastern shore influence
5	Tambor	Golfo de Nicoya	2/17/25	18:55	9.7085	84.9223	Inner gulf, Nicoya Peninsula coast
6	Hermosa offshore	Offshore	2/18/25	14:17	9.3092	84.8911	Offshore central Pacific, ∼30 km from coast
7	Parrita offshore	Offshore	2/18/25	15:29	9.2213	84.7410	Offshore central Pacific, shelf edge
8	Savegre offshore	Offshore	2/18/25	17:45	9.0868	84.4271	Offshore central Pacific, productive waters
9	Quepos offshore	Offshore	2/18/25	19:57	9.2665	84.4682	Offshore Quepos, sportfising grounds
10	Savegre	Coastal	2/19/25	12:56	9.2079	84.0532	Nearshore, Savegre River influence
11	Sierpe	Coastal	2/19/25	14:29	8.8823	83.8730	Nearshore, Sierpe River plume
12	Bajo del Diablo	Coastal	2/19/25	15:46	8.7078	83.9085	Nearshore, Osa Peninsula approach
13	Salsipuedes	Coastal	2/19/25	19:00	8.3744	83.7015	Nearshore southern Pacific
14	Matapalo	Coastal	2/19/25	21:28	8.3235	83.2818	Nearshore, outer Osa Peninsula
15	Boca Golfo	Coastal	2/20/25	13:46	8.3499	83.1747	Golfo Dulce entrance
16	Coto	Golfo Dulce	2/20/25	15:09	8.5557	83.1767	Inner Golfo Dulce, Coto River influence
17	Cocodrilo	Golfo Dulce	2/20/25	15:48	8.5388	83.2615	Inner Golfo Dulce, deep basin
18	Golfito	Golfo Dulce	2/20/25	16:39	8.6088	83.1865	Mid Golfo Dulce, port of Golfito
19	Rincón	Golfo Dulce	2/20/25	17:00	8.7008	83.4289	Outer Golfo Dulce, western shore
20	Esquinas	Golfo Dulce	2/20/25	18:00	8.7039	83.3557	Outer Golfo Dulce, Esquinas sector
21	Sierpe costera	Coastal Return	2/21/25	14:35	8.8113	83.8242	Nearshore return, Sierpe region
22	Quepos costera	Coastal Return	2/21/25	16:42	9.3990	84.2079	Nearshore return, Quepos region
23	Parrita costera	Coastal Return	2/21/25	18:06	9.4037	84.5111	Nearshore return, Parrita region

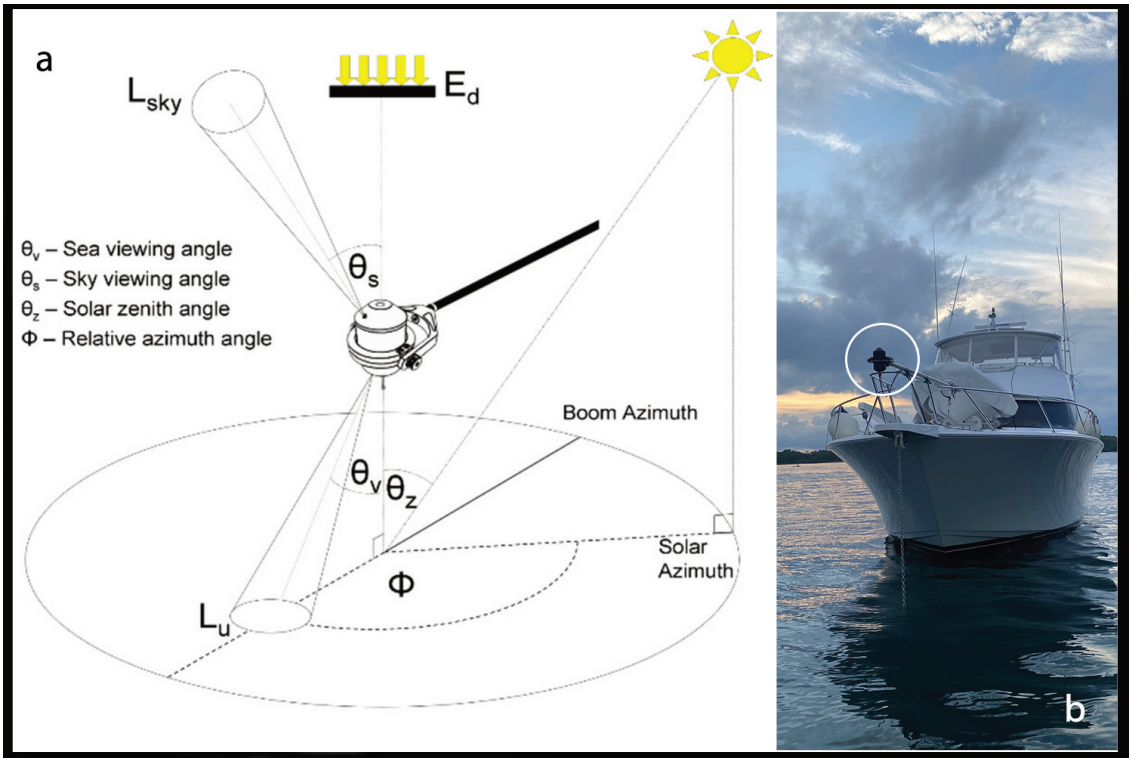


Figure 3.1. DALEC system and deployment configuration. *(a)* Technical schematic of DALEC sensor head showing the three radiometric channels (L_u, L_{sky}, E_d) and motorized azimuth mount with passive gimbal stabilization. *(b)* DALEC bow-mount installation on the M/V *Amejaye*, showing the forward-projecting aluminum pole and sensor positioning approximately 3 m above the sea surface. Schematic source: Brando et al. (2016).

across 340–970 nm for ocean color applications, with NIST-traceable radiometric calibration.

The three radiometric channels measure:

- **Water-leaving radiance (L_u):** Upwelling radiance at 40° from nadir with a 5° field-of-view
- **Sky radiance (L_{sky}):** Downwelling radiance from the sky dome at 40° from zenith with 5° FOV, used to correct for surface-reflected skylight
- **Downwelling irradiance (E_d):** Total downwelling irradiance measured using a fused silica cosine collector with <3% cosine error from 0–60° incidence angles

All three channels sample independently at rates up to 5 Hz with 16-bit analog-to-digital conversion and automatic integration time adjustment (1–6600 ms range).

3.3.3 Deployment Configuration

The DALEC sensor head was mounted on the bow of the *Amejaye*, approximately 3 m above the water surface on an aluminum pole extending ∼1 m forward from the bow (Fig 3.1). This forward-looking bow mount configuration minimizes contamination from ship shadow and superstructure reflection (Zibordi et al., 2004; Brando et al., 2016).

3.3.4 Operational Protocols

The DALEC operated in continuous automatic mode during daylight hours when the vessel was underway and environmental conditions permitted. Following established protocols for above-water radiometry (Mobley, 1999; Hooker et al., 2002), data acquisition was suspended during low sun angle periods (solar zenith angles >60°), high-speed transits (>12 knots), port calls, and periods of rain or

rough seas.

The motorized azimuth control maintained the sensor at $\varphi = 135°$ relative azimuth from the solar plane (the "135° protocol" recommended by Mobley 1999), with a minimum of $\varphi > 90°$ to avoid sunglint.

3.3.5 Remote Sensing Reflectance Derivation

Remote sensing reflectance (R_{rs}, sr^{-1}) was calculated from DALEC-measured radiances and irradiances following standard above-water radiometry protocols (Mobley, 1999):

$$R_{rs}(\lambda) = \frac{L_u(\lambda) - \rho \cdot L_{sky}(\lambda)}{E_d(\lambda)} - \varepsilon \qquad (3.1)$$

where $L_u(\lambda)$ is the measured upwelling radiance, $L_{sky}(\lambda)$ is the measured sky radiance, $E_d(\lambda)$ is the measured downwelling irradiance, ρ is the air–sea interface reflection coefficient, ε is the residual sun and sky glint term, and λ represents wavelength. The ρ depends on sea surface roughness (wind speed), solar zenith angle, viewing geometry, and cloud conditions (Mobley, 1999, 2015).

3.3.6 Data Processing and Quality Control

Raw DALEC data were processed using HyperCP (Hyperspectral Data Processing Software for Ocean Color; Aurin et al. 2024) version 1.2.13, following NASA ocean color validation protocols for above-water radiometry. HyperCP applies a comprehensive processing chain including dark current correction, radiometric calibration, spectral interpolation, motion and tilt corrections, surface reflection correction, residual glint removal, and quality filtering.

3.3.7 Data Archiving

Processed DALEC remote sensing reflectance data, along with comprehensive metadata, were submitted to NASA's SeaBASS (SeaWiFS Bio-optical Archive and Storage System), ensuring long-term accessibility for satellite validation and algorithm development.

3.4 PACE Satellite Observations

3.4.1 PACE Mission Overview and Ocean Color Instrument

The PACE mission, launched by NASA in February 2024, provides hyperspectral ocean color measurements at continuous spectra from the ultraviolet to near-infrared (340–890 nm at 5 nm resolution) plus seven discrete shortwave infrared bands, at 1 km spatial resolution with daily global coverage. The OCI's hyperspectral capability enables discrimination of phytoplankton functional types, detection of HAB species, improved atmospheric correction in coastal waters, and enhanced retrieval of biogeochemical properties in optically complex environments.

3.4.2 PACE Validation Objectives for Pacific Color

The Pacific Color campaign addressed specific validation needs for PACE products in tropical coastal and estuarine waters, characterized by optical complexity, atmospheric correction challenges, spatial heterogeneity, and limited availability of *in situ* validation data. Specific approaches included: construction of a comprehensive matchup dataset; atmospheric correction validation; hyperspectral algorithm development; and a multi-scale validation framework using PACE (1 km), AVIRIS-3 (4 m), DALEC (<1 m), and *in situ* point measurements.

3.4.3 PACE Overpass Coordination and Matchup Criteria

PACE's sun-synchronous orbit provides daily overpasses of the Costa Rica study region at approximately 1300 local time (1900 GMT). The campaign cruise plan maximized stations within optimal temporal windows: 9 stations within ±1 h, 7 stations within ±2 h, and 7 stations within ±3 h of PACE overpass. Standard spatial matchup criteria follow Bailey and Werdell (2006) and Werdell and Bailey (2005).

3.4.4 PACE Data Products and Processing

PACE Level-2 ocean color data products for the study region were obtained from NASA's Ocean Biology Distributed Active Archive Center (OB.DAAC; https://oceancolor.gsfc.nasa.gov/). Standard products include apparent optical properties (R_{rs} at 340–890 nm, $K_d(490)$), biogeochemical products (chlorophyll a, POC, PIC, phytoplankton functional types), and inherent optical properties (a, a_{ph}, a_{dg}, b_{bp}).

3.4.5 Validation Analysis Approach

Validation of PACE ocean color products follows established protocols (Bailey and Werdell, 2006; Werdell and Bailey, 2005; Zibordi et al., 2015), with analyses focused on matchup database construction, spectral validation of R_{rs}, product-specific validation (chlorophyll a, phytoplankton functional types, CDOM), algorithm intercomparison, and uncertainty assessment.

3.4.6 Regional Algorithm Development

Beyond standard validation, the Pacific Color dataset supports development of regional algorithms optimized for tropical coastal waters, including: chlorophyll a retrieval using band ratio, hyperspectral optimization, and machine learning approaches; phytoplankton functional type discrimination including HAB species detection using diagnostic spectral features in PACE hyperspectral data; CDOM retrieval; and turbidity and suspended sediment algorithms. These algorithms can be integrated into FECOP's PezCA mobile application, enabling near-real-time monitoring of ocean conditions and HAB risks.

3.4.7 Airborne Hyperspectral Imagery (AVUELO / AVIRIS-3)

To bridge the spatial gap between localized *in situ* shipboard measurements and satellite-scale footprints, airborne hyperspectral data were incorporated into the analysis. These data were acquired through the Airborne Validation Unified Experiment Land to Ocean (AVUELO), a NASA-led investigation designed to advance the validation of spaceborne hyperspectral observations across tropical ecosystems in Panama and Costa Rica.

During February 2025, the AVUELO campaign deployed the Airborne Visible-Infrared Imaging Spectrometer 3 (AVIRIS-3) (Green et al., 2022) to collect high-resolution hyperspectral imagery. While AVUELO operated as a distinct campaign with comprehensive terrestrial and marine objectives, its flight planning over Costa Rica was coordinated with the Pacific Color 2025 cruise. This collaborative partnership, involving NASA, FECOP, the Smithsonian Tropical Research Institute (STRI), and various academic institutions, enabled simultaneous airborne overflights during the shipboard sampling of the Pacific coastal areas.

This synergistic approach provided a critical intermediate scaling layer for the Plankton, Aerosol, Cloud, ocean Ecosystem (PACE) validation efforts. The aquatic component of the AVIRIS-3 imagery captures fine-scale optical gradients in the coastal zones, estuaries, and offshore transects that are often homogenized within a standard 1×1 km satellite pixel.

The airborne data utilized in this preliminary assessment consist of the provisional AVUELO AVIRIS-3 Orthocorrected Surface Reflectance product (Brodrick et al., 2025). These reflectance data will be evaluated alongside the shipboard DALEC radiometry and HPLC pigment datasets to assess nearshore atmospheric correction performance and spatial heterogeneity.

3.5 Water Sample Collection

3.5.1 Phytoplankton Pigments Analyzed by HPLC

Duplicate and triplicate water samples were filtered through 25 mm GF/F filters (nominal pore size 0.7 µm) under low vacuum pressure (<5 psi). Filtration volumes ranged from 0.5 to 1.0 liters depending on particulate load. Filters were imme-

diately flash-frozen and stored in liquid nitrogen, then shipped frozen to NASA Goddard Space Flight Center (GSFC) for HPLC analysis.

Pigment analysis was performed following Van Heukelem and Thomas (2001) using an Agilent RR1200 HPLC system equipped with a photodiode array detector, refrigerated autosampler, and a C8 reverse-phase column (4.6 × 150 mm Eclipse XDB, 3.5 µm particle size) maintained at 60°C. A two-solvent methanol-based gradient mobile phase was used, with chromatographic output quantified at 450 and 665 nm. Thirty-six peaks were resolved, yielding 26 reported pigments spanning primary, secondary, and tertiary pigment classes (Table 3.2).

The facility operates under a formal quality assurance plan (QAP). Instrument precision averages 0.5% CV for TChl *a* and 1.8% for primary pigments. Replicate sample precision benchmarks for ocean color validation are 5% for TChl *a* and 8% for primary pigments. Replicate precision for Pacific Color 2025 is assessed in Section A.2.1.

Phytoplankton community size structure was estimated from HPLC diagnostic pigment concentrations following Claustre (1994) and Vidussi et al. (2001) as implemented by Uitz et al. (2006), partitioning the community into microplankton (>20 µm), nanoplankton (2–20 µm), and picoplankton (<2 µm) based on fractional contributions of seven diagnostic pigments to the total diagnostic pigment pool [DP]:

$$F_{\text{Micro}} = \frac{[\text{Fuco}] + [\text{Perid}]}{[\text{DP}]} \tag{3.2}$$

$$F_{\text{Nano}} = \frac{[\text{Hex-fuco}] + [\text{But-fuco}] + [\text{Allo}]}{[\text{DP}]} \tag{3.3}$$

$$F_{\text{Pico}} = \frac{[\text{TChl}\,b] + [\text{Zea}]}{[\text{DP}]} \tag{3.4}$$

where [DP] = [Fuco] + [Perid] + [Hex-fuco] + [But-fuco] + [Allo] + [TChl *b*] + [Zea] following Table 3.2. All pigment concentrations are expressed in mg m^{-3}. Below-detection-limit values were treated as zero, consistent with standard practice.

Additional water sample analyses included:

Chromophoric Dissolved Organic Matter (CDOM): At a subset of stations, water samples were filtered through 0.2 µm syringe filters and stored refrigerated in dark glass bottles. CDOM absorption spectra were measured at NASA GSFC using a spectrophotometer across 250–750 nm.

Inorganic Nutrients: Duplicate samples for nitrate, nitrite, ammonium, and phosphorus were collected in 15 mL polyethylene bottles, passed through a 0.45-µm Swinnex filter and kept in the dark at 4 °C until analysis. Their concentrations were measured at UNA using a SCAN++ (Skalar) autoanalyzer following the method described by Hansen and Koroleff (2007).

Chlorophyll (Chl): Surface water samples were collected at each monitoring station in duplicate using dark bottles to minimize light exposure and handled carefully to avoid bubble formation, thereby limiting biological activity within the sample containers. Sample volumes ranged from 1 to 2 L, depending on water color at each sampling site. Immediately after collection, samples were filtered through 47-mm GF/F glass fiber filters using a vacuum filtration system. After filtration, each filter was folded in half with the pigmented side facing inward, folded repeatedly, wrapped in aluminum foil, labeled, and stored under refrigerated conditions until laboratory analysis. The filtered water volume was recorded for each sample. Chlorophyll analyses followed the methodology of American Public Health Association et al. (1999), consisting of pigment extraction with 90% acetone followed by absorbance measurements using spectrophotometry.

Microplastics: Triplicate surface-water samples were collected and for each replicate, 1 L of seawater was filtered through a 63-µm mesh sieve, and the retained material was transferred into glass vials for subsequent analysis. In the laboratory, samples were transferred to previously washed, sterilized, and dried Petri dishes to minimize airborne contamination. Each dish was covered with aluminum foil perforated with small holes and placed in a drying oven to allow water evaporation, leaving

the particles at the bottom of the dish. A particle was classified as a microplastic if it met the following criteria: 1) It lacked recognizable cellular structures. 2) It shrank or melted when touched with a heated needle. 3) In the case of fibers, the color and thickness were uniform, and the fibers did not break apart or disintegrate when handled (Balla et al., 2024). Each microplastic particle was counted, measured (mm), classified according to its morphology (fragment, fiber, film, or pellet) and color (transparent/translucent, blue, red, yellow, black, or green), and photographed.

Total Carbon and Heavy Metals: Twenty-three surface seawater samples were collected and each sample was divided into two subsamples. From each sample, one subsample was preserved with concentrated nitric acid (HNO_3) and stored at 4 °C (Hasan et al., 2023) for heavy metal analysis, while the other was treated with hydrochloric acid (HCl) to remove inorganic carbon prior to analysis (Shetty and Goyal, 2022) and was stored at 4 °C. Heavy metal analyses were conducted using atomic absorption spectrometry (Thermo Scientific iCE 3000 Series). Copper (Cu), nickel (Ni), and zinc (Zn) were quantified using flame atomization, whereas cadmium (Cd) and lead (Pb) were analyzed using graphite furnace atomization. Before analysis, all samples underwent microwave-assisted nitric acid digestion. At the time of writing this report, total carbon samples were still pending laboratory processing.

Prokaryotic and Eukaryotic Community Structure:

DNA Extraction and Sequencing: Water samples (1 L) were sequentially filtered through a 20 µm mesh onto 3 µm and then 0.2 µm polycarbonate filters and frozen in liquid nitrogen; DNA was later extracted with the phenol-chloroform protocol following Massana et al. (1997). The 515F-Y and 926R primers (Parada et al., 2016) and the V4_Balzano primer (Balzano et al., 2015) were used to generate amplicons targeting the V4 region of the prokaryotic 16S rRNA gene and the eukaryotic 18S rRNA gene, respectively.

3.6 Phytoplankton Sampling and Identification

3.6.1 Net Tow Sampling

Surface phytoplankton samples were collected at each station using a 25-µm mesh plankton net deployed for approximately one minute in surface waters. The concentrated sample from the cod end was transferred to pre-labeled collection bottles containing formalin fixative ($n = 25$ total net samples across the campaign). The 25-µm mesh captures microplankton (>20 µm) including larger diatoms, dinoflagellates, and chain-forming species, complementing the quantitative Niskin bottle samples.

3.6.2 Niskin Bottle Water Samples

Discrete water samples were collected at each station using (1) a bucket for surface water (0 m) and (2) a 1.7-liter Niskin bottle deployed to approximately 5 m depth. A total of 45 Niskin samples were collected across all stations, preserved with basic Lugol's iodine solution for subsequent cell enumeration using inverted microscopy.

3.6.3 Field Observations and Live Microscopy

At each station, detailed field observations were recorded including time, weather conditions, water color, and other notable characteristics. Between stations, a field microscope was set up in the vessel's interior to examine fresh aliquots from each sample, enabling preliminary assessment of phytoplankton community composition using reference literature.

3.6.4 Sample Processing and Laboratory Analysis

Following the campaign, all samples were transported to UCR for comprehensive analysis (ongoing at the time of this report). Laboratory processing involves multiple stages:

Table 3.2. Photosynthetic phytoplankton pigments and their sums analyzed at the NASA GSFC HPLC facility. Primary, secondary, and tertiary pigments are shown with their variable forms, names, and calculations. Abbreviations are shown in parentheses.

Pigment / Sum	**Calculation**
Primary Pigments	
Total chlorophyll *a* (TChl *a*)	[Chlide *a*] + [DVChl *a*] + [MVChl *a*]
Total chlorophyll *b* (TChl *b*)	[DVChl *b*] + [MVChl *b*]
Total chlorophyll *c* (TChl *c*)	[Chl c_1] + [Chl c_2] + [Chl c_3] + [MGDVP]
Carotenes (Caro)	[β,β-Car] + [β,ε-Car]
Alloxanthin (Allo)	—
19′-Butanoyloxyfucoxanthin (But-fuco)	—
Diadinoxanthin (Diad)	—
Diatoxanthin (Diato)	—
Fucoxanthin (Fuco)	—
19′-Hexanoyloxyfucoxanthin (Hex-fuco)	—
Peridinin (Perid)	—
Zeaxanthin (Zea)	—
Secondary Pigments	
Monovinyl Chlorophyll *a* (MVChl *a*)	[MVChl *a*] + [allomers] + [epimer]
Divinyl Chlorophyll *a* (DVChl *a*)	[DVChl *a*] + [allomers] + [epimer]
Chlorophyllide *a* (Chlide *a*)	—
Monovinyl Chlorophyll *b* (MVChl *b*)	[MVChl *b*] + [epimer]
Divinyl Chlorophyll *b* (DVChl *b*)	[DVChl *b*] + [epimer]
Chlorophyll $c_1 + c_2$ (Chl c_{1+2})	[Chl c_1] + [Chl c_2] + [MGDVP]
Chlorophyll c_3 (Chl c_3)	[Chl c_3] + [MVChl c_3]
Tertiary Pigments	
Lutein (Lut); Neoxanthin (Neo); Violaxanthin (Viol)	—
Pheophytin *a* (Phytin *a*)	[Phytin *a*] + [Phytin *a* allomer]
Pheophorbide (Phide *a*)	Sum of up to 5 Phide *a* pigments
Prasinoxanthin (Pras)	—
Pigment Sums	
Total Chlorophyll (TChl)	[TChl *a*] + [TChl *b*] + [TChl *c*]
Photoprotective Carotenoids (PPC)	[Allo] + [Diad] + [Diato] + [Zea] + [Caro]
Photosynthetic Carotenoids (PSC)	[But] + [Fuco] + [Hex] + [Peri]
Photosynthetic Pigments (PSP)	[PSC] + [TChl]
Total Carotenoids (TCaro)	[PPC] + [PSC]
Total Accessory Pigments (TAcc)	[PPC] + [PSC] + [TChl *b*] + [TChl *c*]
Total Diagnostic Pigments (DP)	[PSC] + [Allo] + [Zea] + [TChl *b*]

Concentration and settling: Samples are transferred to 250 or 500 mL graduated cylinders and settled for a minimum of 24 hours. From initial volumes of ∼500 mL, samples are concentrated to final volumes of ∼10 mL in properly cataloged vials.

Formalin-fixed net samples ($n = 25$): Taxonomic identification to the lowest practical level (typically species or genus), with particular attention to HAB species. High-resolution photographic documentation is provided for major taxa, with selected specimens prepared for scanning electron microscopy.

Lugol-fixed Niskin samples ($n = 45$): Analyzed using inverted microscopy following the Utermöhl sedimentation technique. Quantitative enumeration yields cell concentrations in cells L^{-1}, with biovolume estimates enabling phytoplankton carbon biomass assessment.

3.6.5 Data Products and Timeline

Phytoplankton analysis is ongoing at UCR as of this report. Planned data products include taxonomic species lists, quantitative cell concentrations (cells L^{-1}), phytoplankton biovolume and estimated carbon biomass, high-resolution microphotographs, scanning electron microphotographs, comparison with HPLC pigment-based estimates, and HAB species presence and abundance assessment.

3.7 Oceanographic Measurements

3.7.1 CTD Profiling

At each station, vertical profiles of temperature, salinity, and pH were acquired using a handheld CTD profiler, slowly lowered through the upper water column to capture near-surface stratification structure, thermocline depth, and vertical variability in water properties.

3.7.2 Water Transparency

Water transparency was measured at each station using a standard Secchi disk, lowered on the shaded side of the vessel. The Secchi depth was recorded as the average of the disappearance and reappearance depths, providing an integrated measure of water clarity and enabling comparison with historical datasets.

3.8 Zooplankton and Fish Larvae Sampling

Vertical net tows for zooplankton and ichthyoplankton collection were conducted at a subset of five stations (Stations 8, 9, 13, 19, and 21) using a 500 µm mesh plankton net deployed to depths of approximately 70–90 m and hauled vertically over 2–4 minutes. Collected material was immediately preserved in ethanol or formalin for subsequent taxonomic identification and abundance estimation. Preliminary results from ichthyoplankton analysis are presented in Section 4.5; zooplankton analysis is ongoing and results will be incorporated in a subsequent version of this report.

4. Preliminary Results

4.1 General Oceanographic Observations

4.1.1 Surface Hydrography

Surface temperature, salinity, pH, and water transparency measurements revealed clear spatial patterns across the study region (Fig 4.1).

Temperature was relatively uniform, ranging from 27.5°C to 30.3°C (mean 29.2 ± 0.6°C). The coolest water was observed at **Stn. 4** (Paquera, 27.5°C) in the mid-Gulf of Nicoya, while the warmest occurred at **Stn. 20** (Esquinas, 30.3°C) in the inner Golfo Dulce. Regional averages: Gulf of Nicoya (28.4°C), offshore (29.3°C), coastal (29.2°C), and Golfo Dulce (29.8°C).

Salinity exhibited strong spatial gradients reflecting freshwater influence and estuarine–oceanic mixing. The lowest salinity was measured at **Stn. 16** (Coto, 29.87 PSU) in Golfo Dulce near the Coto River mouth, while the highest occurred at **Stn. 9** (Quepos offshore, 32.49 PSU). Regional

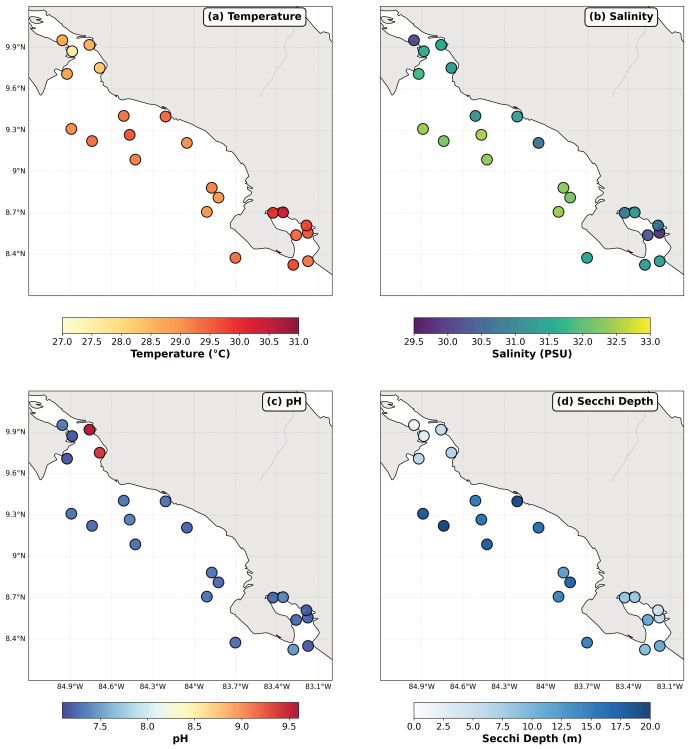


Figure 4.1. Surface hydrographic observations across the Pacific Color 2025 cruise track. Spatial distributions of (a) sea surface temperature, (b) surface salinity, (c) surface pH, and (d) Secchi depth for all 23 stations. Station symbols are colored by transect region.

patterns were distinct: Gulf of Nicoya (31.3 PSU), offshore (32.4 PSU), coastal (31.6 PSU), and Golfo Dulce (30.6 PSU).

pH showed marked spatial variability. Stations 1 (Tárcoles) and 2 (Caldera) in the outer Gulf of Nicoya exhibited pH values of 9.4 and 9.55, respectively, substantially elevated above normal seawater pH (∼8.1–8.3). The remainder of the campaign showed pH ranging from 7.17 to 7.48 (mean 7.29 ± 0.09, excluding the two anomalous stations).

The elevated pH values at Stations 1–2 may reflect multiple interacting factors. Intense photosynthetic activity removing CO_2 from surface waters creates diel patterns commonly observed in productive coastal environments. However, these stations are also strongly influenced by Tárcoles River discharge from Costa Rica's densely populated Central Valley. The pH values of 9.4–9.55 fall within the range identified as optimal for harmful cyanobacterial bloom development (Wei et al., 2022) and conducive to elevated haptophyte toxicity (Prosser et al., 2012). Recent studies have shown that pH plays a critical role in regulating HAB dynamics and toxicity: Wei et al. (2022) reported that optimal pH for *Microcystis aeruginosa* proliferation was 9.55, while Liu et al. (2016) found that pH-dependent inorganic carbon speciation strongly influences algal growth rates.

Stn. 3 (San Lucas, pH 7.34) exhibited intensely green, malodorous water (field notes indicate "strong smell from net"), possibly reflecting elevated respiration or recent senescence. Stations 4–5, sampled later in the day (1739–1855 GMT), showed pH values of 7.18 and 7.17, likely reflecting the transition from net autotrophy to heterotrophy as afternoon progressed.

Secchi depth varied by more than 20-fold across the study area, from 0.9 m at **Stn. 3** (San Lucas) to 19.5 m at **Stn. 7** (Parrita offshore). Gulf of Nicoya stations ranged from 0.9 m to 7.0 m (mean 4.5 m). Offshore stations exhibited the greatest transparency (mean 17.6 m, range 15.5–19.5 m). Coastal stations showed intermediate values (mean 13.5 m, range 9–17 m). Golfo Dulce displayed moderate to low transparency (mean 7.2 m, range 3.5–11 m), with the most turbid water at **Stn. 18** (Golfito, 3.5 m) and **Stn. 16** (Coto, 5.5 m).

4.1.2 Surface Nutrient Distributions

Surface water nutrient concentrations revealed substantial spatial variability across the study region (Fig 4.2).

Gulf of Nicoya: Gulf surface nutrients (**Stn. 1**–**Stn. 5**) were moderate during late dry season sampling, with nitrate ranging 0.16–1.18 µmol L^{-1}, phosphate 0.23–0.40 µmol L^{-1}, and silicate 0.47–5.43 µmol L^{-1}. Ammonium (3.18–3.82 µmol L^{-1}) exceeded nitrate throughout, indicating dominance of regenerated nitrogen. These concentrations are notably lower than historical measurements (Palter et al., 2007; Kress et al., 2002), likely reflecting late dry season timing, station positioning in the

outer to mid-gulf, and dilution with lower-nutrient coastal waters. Low N:P ratios (DIN:PO_4^{3-} = 9:1 to 17:1 vs. Redfield 16:1) suggest potential nitrogen limitation, consistent with Kress et al. (2002).

Offshore and coastal waters: Offshore stations (**Stn. 6**–**Stn. 9**) exhibited low nutrient concentrations characteristic of oligotrophic tropical surface waters (nitrate 0.03–0.49 µmol L^{-1}, phosphate 0.50–0.86 µmol L^{-1}). **Stn. 8** (Savegre offshore) showed anomalously low nitrate (0.03 µmol L^{-1}) despite the campaign's highest ammonium (9.25 µmol L^{-1}), possibly reflecting localized remineralization. Coastal stations (**Stn. 10**–**Stn. 15**, **Stn. 21**–**Stn. 23**) showed variable but generally low nutrients. **Stn. 11** (Sierpe), positioned close to the Sierpe River mouth, shows clear riverine influence with elevated silicate (3.96 µmol L^{-1}) but low phosphate (0.19 µmol L^{-1}), consistent with pristine forested watershed drainage.

Golfo Dulce: Golfo Dulce stations (**Stn. 16**–**Stn. 20**) exhibited distinctive patterns reflecting unique fjord circulation. Surface nitrate was uniformly low (0.002–0.27 µmol L^{-1}). The most salient feature was exceptionally high silicate at **Stn. 16** (Coto, 10.46 µmol L^{-1}), nearly double any other campaign value, possibly indicating Coto River input from the forested interior. Ammonium was elevated at **Stn. 18** (Golfito, 5.13 µmol L^{-1}), which could reflect anthropogenic influence from the Golfito harbor.

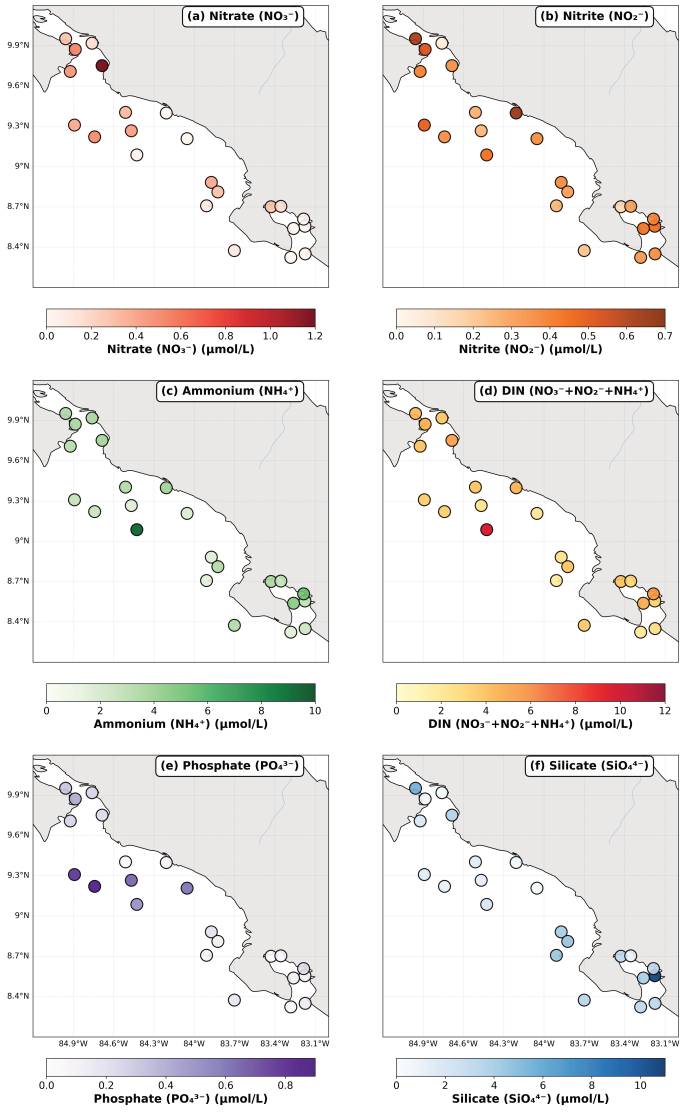


Figure 4.2. Surface nutrient distributions across the Pacific Color 2025 cruise track. Concentrations (µmol L^{-1}) of (a) nitrate, (b) ammonium, (c) phosphate, and (d) silicate at all 23 stations.

4.2 Additional Water Measurements

Microplastics:

Microplastics were detected at all sites, with mean abundances ranging from 5.33 particles L^{-1} at Tambor to 48 particles L^{-1} in the Quepos Offshore area. Particles were approximately 1 mm in size at most sampling stations but were larger on average at Tárcoles (4.60 mm) and Caldera (4.43 mm). Translucent and blue fibers predominated, with fewer red particles, fragments, and films. Fiber-type particles were also dominant, with few fragments and films observed.

Heavy Metals:

Neither copper (Cu < 0.6 mg L^{-1}) nor lead (Pb < 0.0016 mg L^{-1}) was detected, whereas cadmium (Cd) and nickel (Ni) were detected in all samples, but at very low concentrations. Zinc (Zn) was detected in 9 of the 23 samples.

4.3 Phytoplankton Pigment Distributions

Surface phytoplankton pigment concentrations measured by HPLC revealed strong spatial gradients across the study area (Fig 4.3). Total chlorophyll *a* (TChl *a*), used here as a proxy for total phytoplankton biomass, ranged from 0.20 mg m^{-3} at oligotrophic offshore stations to 8.13 mg m^{-3} at **Stn. 3** (San Lucas, inner Gulf of Nicoya). To quantify community composition shifts, we applied the diagnostic pigment approach of Uitz et al. (2006) (Equations 3.2–3.4) to partition the community into microplankton, nanoplankton, and picoplankton size fractions (Fig 4.4).

4.3.1 Gulf of Nicoya

The Gulf of Nicoya stations showed the highest biomass of the campaign (TChl *a*: 1.4–8.1 mg m^{-3}, peaking at **Stn. 3**), strongly dominated by microplankton (F_{Micro}: 0.64–0.88). Fucoxanthin and Peridinin dominated the diagnostic pigment signal, pointing to diatoms and dinoflagellates, corroborated directly by cell counts (Section 4.4.4) at Tárcoles (**Stn. 1**: *Chaetoceros curvisetus*, *Thalassionema nitzschioides*), Caldera (**Stn. 2**: mixed diatom–dinoflagellate assemblage including *Tripos* spp. and *Alexandrium monilatum*), and Tambor (**Stn. 5**: *Tripos* spp. dominating).

Stn. 3 (San Lucas) stood out as the most productive site (TChl *a*: 8.1 mg m^{-3}), visually confirmed by markedly green water, a strong odor from the phytoplankton net, and a Secchi depth of 0.9 m. The progressive increase in F_{Pico} from **Stn. 1** to **Stn. 5** (0.117 → 0.241) and decrease in F_{Micro} (0.821 → 0.643) suggests a gradual transition toward smaller cells as nutrient concentrations taper off toward the open coast. Peridinin was notably elevated at **Stn. 2** (Caldera, ∼0.90 mg m^{-3}) and **Stn. 4** (Paquera, ∼0.44 mg m^{-3}).

4.3.2 Offshore Stations

The four offshore stations (**Stn. 6**–**Stn. 9**) displayed the lowest phytoplankton biomass of the campaign (TChl *a*: 0.25–0.46 mg m^{-3}), representing a sharp biological transition from the productive Gulf of Nicoya. Picoplankton dominated across all four stations (F_{Pico}: 0.61–0.79), with Zeaxanthin and TChl *b* as the leading diagnostic pigments, reflecting dominance of cyanobacteria (*Synechococcus* and *Prochlorococcus*) in nutrient-depleted offshore waters. Microplankton fractions were the lowest recorded (F_{Micro}: 0.08–0.21).

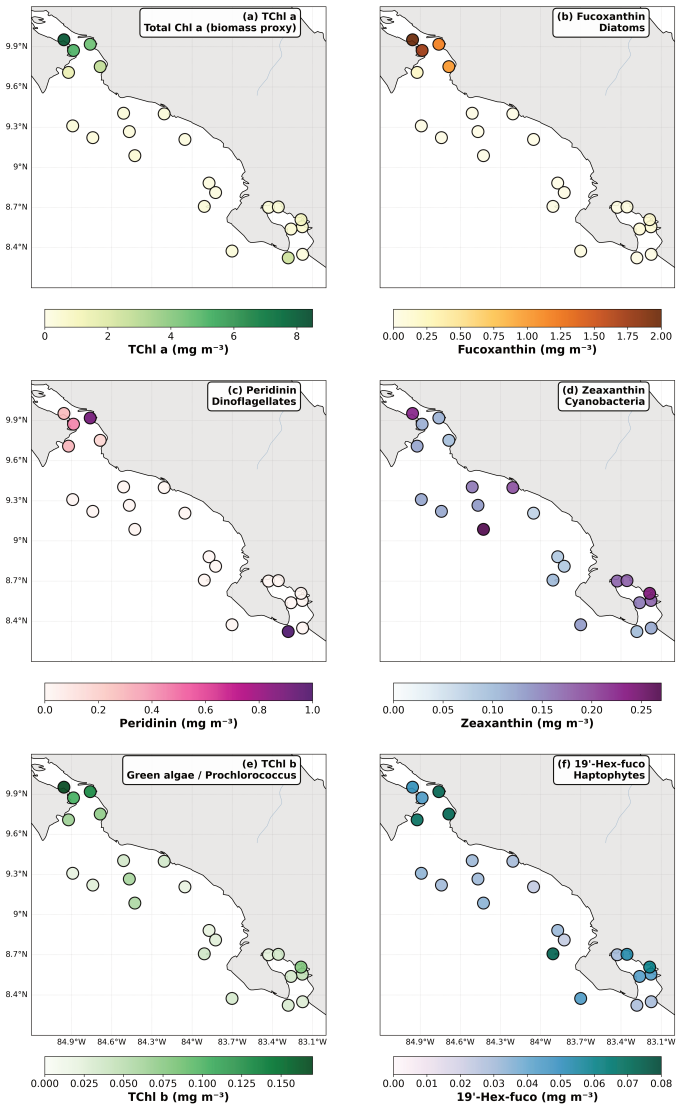


Figure 4.3. Surface phytoplankton pigment distributions. (a) Total chlorophyll *a* (TChl *a*, mg m^{-3}) and (b–f) selected diagnostic carotenoid concentrations at all 23 stations along the Pacific Color 2025 cruise track.

4.3.3 Coastal Stations

Coastal stations (**Stn. 10**–**Stn. 15**) showed the most variable community structure of the campaign (TChl *a*: 0.20–2.44 mg m^{-3}), with most stations dominated by picoplankton (F_{Pico}: 0.52–0.67). **Stn. 12** recorded the highest nanoplankton fraction of the campaign ($F_{Nano} = 0.33$), suggesting a localized haptophyte or cryptophyte signal.

Stn. 14 (Matapalo) was the most anomalous coastal station: TChl *a* reached 2.44 mg m^{-3}, F_{Micro} was the highest of the coastal transect (0.87), and Peridinin reached its campaign maximum (∼1.13 mg m^{-3}, single replicate), indicating a localized dinoflagellate assemblage. This result is based on a single HPLC replicate and should be interpreted with caution (see Section A.2.1).

Stn. 15 (Boca Golfo Dulce) presented a striking example of the complementary and to a significant degree non-overlapping nature of pigment-based and light microscopy approaches. Despite the highest total cell abundance of any counted station (∼415 × 10^3 cells L^{-1}, dominated entirely by *Tripos* spp.; see Section 4.4.4), the pigment-based microplankton fraction was relatively low ($F_{Micro} = 0.156$), with picoplankton dominating the pigment signal ($F_{Pico} = 0.671$). This reflects the differential sensitivity of the two methods: HPLC integrates the pigment signal across the full size spectrum including picoplankton invisible to standard light microscopy, while cell counts are biased toward the larger, microscopically visible microplanktonic taxa.

4.3.4 Golfo Dulce

Golfo Dulce stations (**Stn. 16**–**Stn. 20**) displayed intermediate-to-low biomass (TChl *a*: 0.30–0.80 mg m^{-3}) with picoplankton consistently dominant (F_{Pico}: 0.56–0.73). The highest TChl *a* and microplankton fractions within this region (F_{Micro}: 0.26–0.29) were at Stations 16–18, consistent with terrestrial inputs. **Stn. 16** (Coto) showed visually green water, shallow Secchi depth (5.5 m), reduced salinity (29.87 PSU), and the highest silicate of the campaign (10.46 µmol L^{-1}), all indicative of direct riverine influence capable of supporting diatom growth. No cell count data are available for Golfo Dulce stations.

4.3.5 Coastal Return Transect

The three return coastal stations (**Stn. 21**–**Stn. 23**) showed low biomass (TChl *a*: 0.23–0.37 mg m^{-3}) with strong picoplankton dominance (F_{Pico}: 0.65–0.74) and high Secchi depths (15–19 m), broadly comparable to the offshore and open coastal stations and consistent with an oligotrophic oceanic background signal. No cell count data are available for return coastal stations.

4.4 Phytoplankton Abundance

The spatial distribution of phytoplankton taxa and their qualitative abundance across Stations 1–14 is presented in Fig 4.5, while quantitative cell counts for four stations with completed enumeration are illustrated in Fig 4.8. These should be interpreted jointly as complementary representations at different levels of analytical completion, and alongside the pigment-based size fraction estimates (Fig 4.4).

4.4.1 Taxonomic Composition

A total of 53 phytoplankton taxa belonging to four phytoplankton functional types were identified across surface water samples collected during the campaign (Fig 4.5). Diatoms were the most speciose group with 27 taxa (51% of total), followed by dinoflagellates with 23 taxa (43.4%), cyanobacteria with 2 taxa (3.77%), and silicoflagellates with 1 taxon (1.9%). Together, diatoms and dinoflagellates accounted for 94.4% of the total number of identified taxa, consistent with their well-established co-dominance in tropical coastal phytoplankton assemblages.

Among diatoms, the most diverse and frequently observed genera were *Chaetoceros*, *Coscinodiscus*, *Ditylum*, *Thalassionema* (represented by *T. frauenfeldii* and *T. nitzschioides*), *Thalassiosira*, *Stephanopyxis*, and *Rhizosolenia*. Within

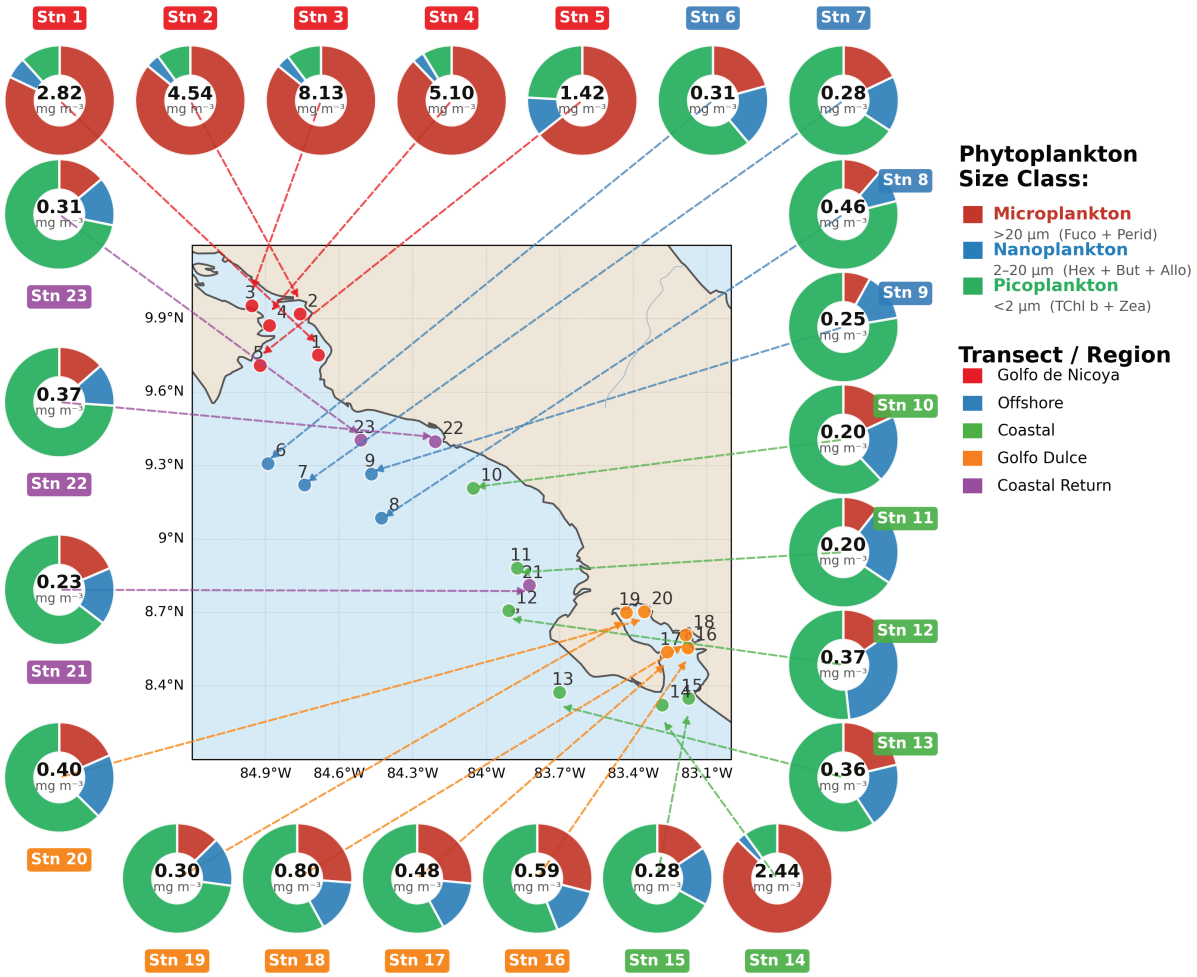


Figure 4.4. Phytoplankton size-fractionated community structure across 23 stations sampled during the Pacific Color campaign (February 17–21, 2025). Ring plots show the relative contribution of microplankton (>20 µm, red), nanoplankton (2–20 µm, blue), and picoplankton (<2 µm, green) estimated from HPLC diagnostic pigments following Uitz et al. (2006) as formulated from Claustre (1994) and Vidussi et al. (2001). Center values indicate TChl *a* (mg m^{-3}). Station markers are colored by transect region: Gulf of Nicoya (red), offshore (blue), coastal (green), Golfo Dulce (orange), coastal return (purple).

dinoflagellates, the most prominent genera were *Tripos* (Fig 4.6) (formerly *Ceratium*; represented by *T. dens*, *T. furca*, *T. fusus*, and *T. cf. gibberum*), *Alexandrium*, *Dinophysis*, *Protoperidinium*, *Akasiwo*, and *Noctiluca*. The cyanobacteria *Trichodesmium erythraeum* (Fig 4.7) and *Gloeotrichia* sp. were also recorded at multiple stations, while the silicoflagellate *Dictyocha fibula* was observed at several nearshore and offshore stations.

Of particular ecological significance is the presence of several harmful algal bloom (HAB)-associated taxa across the study area. *Dinophysis* spp. (four species: *D. caudata*, *D. hastata*, *D. mitra*, and *D. rotundata*), which are associated with diarrhetic shellfish poisoning (DSP), were recorded at multiple stations across the Gulf of Nicoya, offshore, and coastal transects. *Gymnodinium catenatum* and cysts (*quistes*) of *Pyrodinium bahamense*, both producers of paralytic shellfish toxins (PST), were observed at Caldera (**Stn. 2**) and San Lucas (**Stn. 3**) within the Gulf of Nicoya. *Margalefidinium polykrikoides*, associated with harmful fish-killing blooms, was recorded at Tárcoles (**Stn. 1**). *Alexandrium monilatum*, a HAB-forming species

producing bioactive toxins, was among the most widespread dinoflagellates recorded during the campaign, observed at stations spanning all sampled transects. No bloom conditions attributable to any of these HAB taxa were reported in field observations at the time of sampling; however, their widespread occurrence across the study area warrants continued monitoring.



Figure 4.5. Qualitative phytoplankton abundance across 14 stations (Days 1–3). Rows represent individual taxa organized by taxonomic group; columns represent stations ordered along the cruise track. Color intensity indicates qualitative abundance: light green = low abundance; medium green = abundante; dark green = very abundant; white = not observed; gray = not yet analyzed. Row label background colors denote ecological significance: orange = toxic species (HAB-associated, PST or DSP producers); dark orange = harmful species (non-toxin HAB taxa); purple = bioluminescent species. Colored squares above station labels indicate transect. Data for Golfo Dulce (**Stn. 16**–**Stn. 20**) and Coastal Return (**Stn. 21**–**Stn. 23**) are pending.

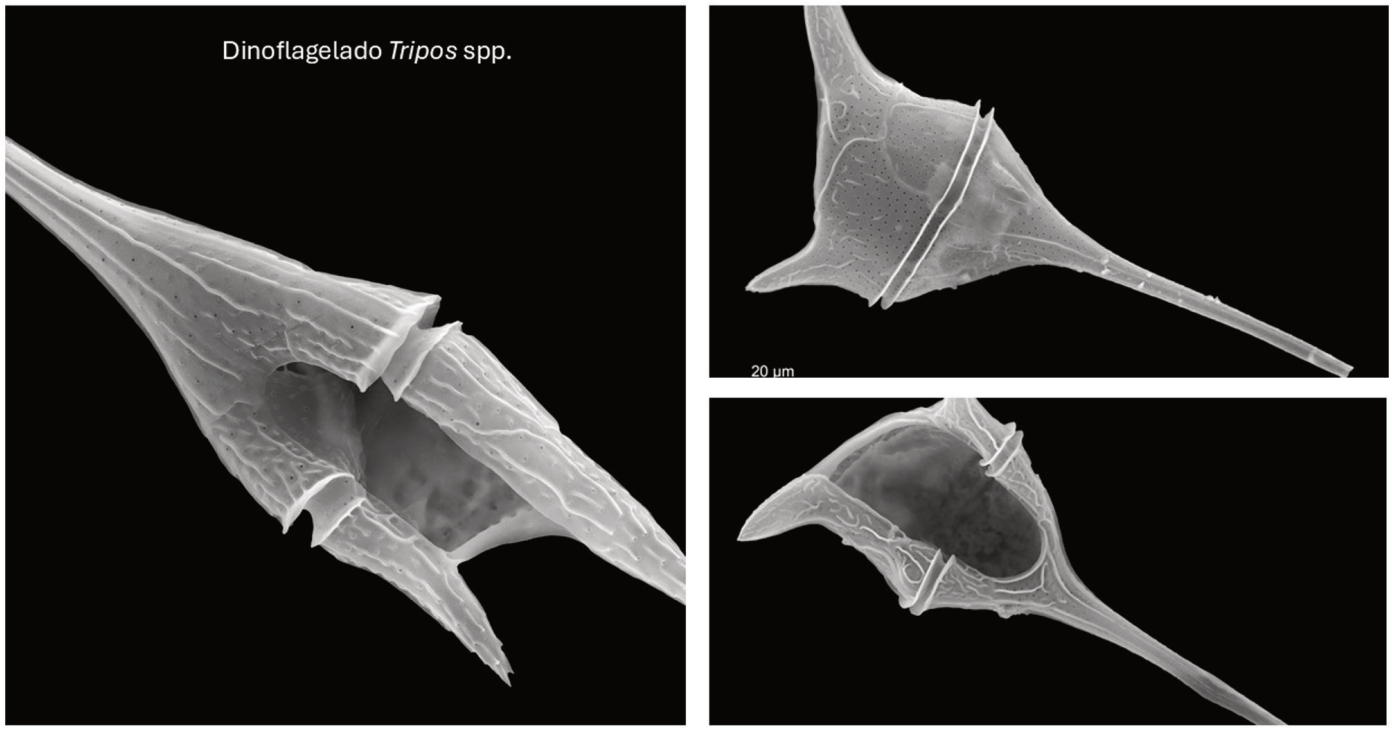


Figure 4.6. Scanning electron microphotographs of *Tripos* spp. collected during the Pacific Color 2025 campaign (February 17–21, 2025), Costa Rican Pacific coast. Characteristic features visible include the heavily ornamented theca, prominent apical horn, and divergent antapical horns diagnostic of the genus. *Tripos* (formerly *Ceratium*) was the most ubiquitous and abundant dinoflagellate genus recorded during the campaign, present at all four quantitatively counted stations (**Stn. 1**, **Stn. 2**, **Stn. 5**, **Stn. 15**) and observed qualitatively across virtually all 23 sampling stations. Scale bars as indicated. SEM microphotographs from M. Vargas, UCR.

4.4.2 Qualitative Abundance Distribution (Days 1–3, Stations 1–14)

Gulf of Nicoya (Stn. 1–Stn. 5). The Gulf of Nicoya exhibited the richest and most diverse assemblages, consistent with high TChl *a* (mean ∼4.40 mg m^{-3}) and strong microplankton dominance (F_{Micro}: 0.64–0.88). **Stn. 3** (San Lucas) was qualitatively the most productive station, with *Coscinodiscus* spp., *Thalassiosira* chains, *Chaetoceros* spp., *Ditylum brightwellii*, *Stephanopyxis turris*, and both *Thalassionema* species all assessed as very abundant, and *Alexandrium monilatum*, *Akasiwo sanguineum*, and *Tripos* spp. also very abundant.

Stn. 1 (Tárcoles) was dominated by diatoms: *Chaetoceros curvisetus* (100×10^3 cells L^{-1}), *Thalassionema nitzschioides* (45×10^3 cells L^{-1}), *Ditylum brightwellii* (15×10^3 cells L^{-1}), and *Coscinodiscus granii* (8×10^3 cells L^{-1}), comprising a total partial count of 168×10^3 cells L^{-1}.

Stn. 2 (Caldera) showed the most taxonomically diverse counted community (272×10^3 cells L^{-1}), with dinoflagellates collectively dominating (∼64%; 175×10^3 cells L^{-1}), led by *Tripos dens* (54×10^3 cells L^{-1}), *Tripos furca* (49×10^3 cells L^{-1}), *Alexandrium monilatum* (45×10^3 cells L^{-1}), *Akasiwo sanguineum* (15×10^3 cells L^{-1}), and *Tripos fusus* (12×10^3 cells L^{-1}). Diatoms contributed ∼36%. Notably, *Gymnodinium catenatum*, cysts of *Pyrodinium bahamense*, and multiple *Dinophysis* species were all recorded as abundant, representing a diverse HAB assemblage warranting attention.

At Tambor (**Stn. 5**), the counted community

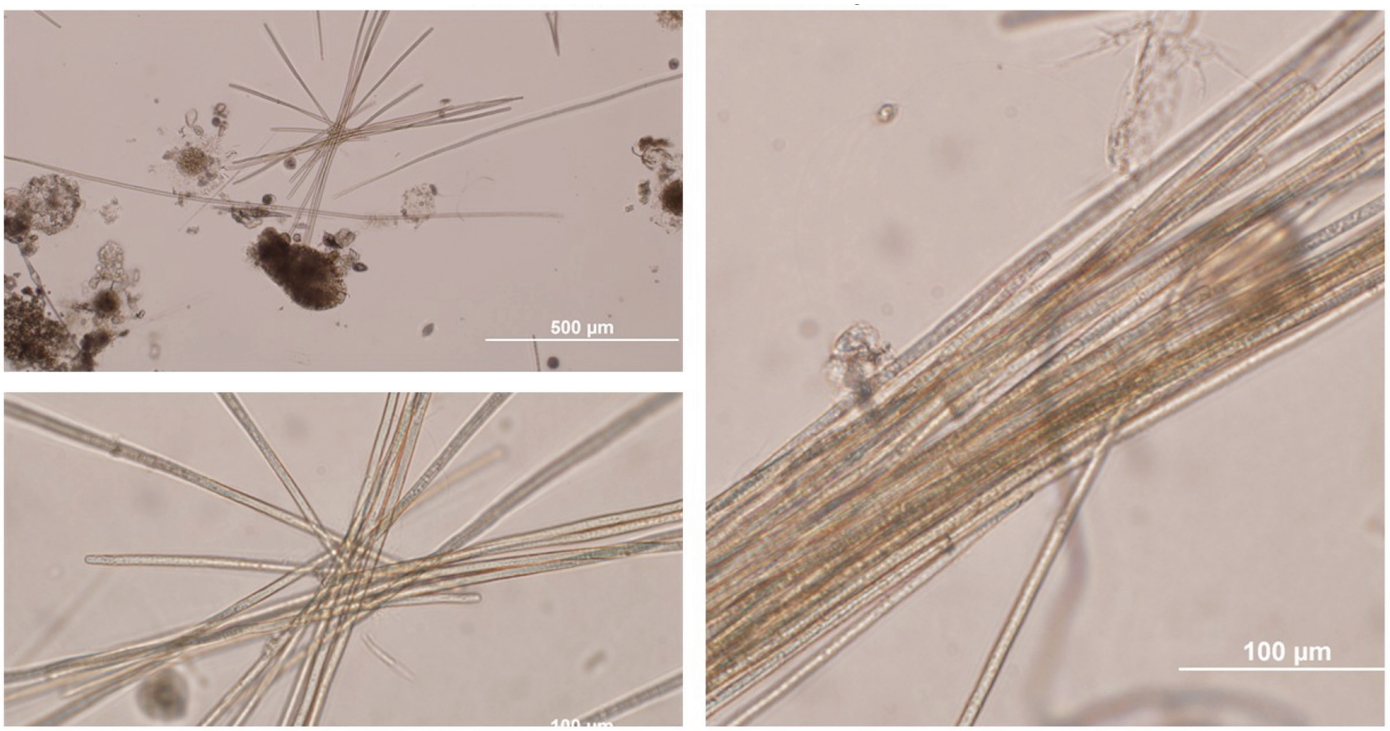


Figure 4.7. Light microphotographs of *Trichodesmium erythraeum* colonies collected during the Pacific Color 2025 campaign. Characteristic trichome bundle morphologies are visible, including puff-shaped (*tuft*) and raft-shaped (*fascicle*) colony arrangements typical of this species. Samples were collected from surface waters during February 17–21, 2025 along the Costa Rican Pacific coast. *T. erythraeum* is a filamentous, nitrogen-fixing cyanobacterium whose presence was detected at multiple stations across the Gulf of Nicoya, coastal, and southern Pacific transects, consistent with the Zeaxanthin signal recorded in HPLC pigment analyses at those stations (photo: M. Vargas, UCR).

was represented by *Tripos* spp. (*T. dens*: 65 × 10^3; *T. furca*: 55 × 10^3; *T. fusus*: 18 × 10^3; total: 138 × 10^3 cells L^{-1}), with additional dinoflagellates and diatoms awaiting enumeration.

Offshore Stations (Stn. 6–Stn. 9). The offshore transect showed a marked reduction in diversity and abundance, consistent with oligotrophic conditions (TChl *a*: 0.25–0.46 mg m^{-3}) and strong picoplankton dominance (F_{Pico}: 0.61–0.79). **Stn. 6** (Hermosa) was the most diverse offshore station, with *Chaetoceros* spp., *Ditylum brightwellii*, *Thalassiosira* colonial chains, and *Dictyocha fibula* all recorded as abundant. HAB taxa including *Alexandrium monilatum* and *Dinophysis* spp. were recorded at Hermosa and Parrita despite oligotrophic conditions.

Coastal Stations (Stn. 10–Stn. 14). Coastal stations showed generally low abundance and diversity (F_{Pico}: 0.52–0.67). **Stn. 13** (Salsipuedes) emerged as a noteworthy hotspot, with chain-forming *Tripos* spp. as very abundant and *Trichodesmium erythraeum* as abundant. **Stn. 14** (Matapalo) showed only diatoms (*Chaetoceros* spp., *Ditylum brightwellii*, *Thalassionema nitzschioides*) in qualitative assessment, despite the highest Peridinin concentration of the campaign, likely reflecting the preliminary and incomplete nature of qualitative assessment at this station.

4.4.3 Cyanobacteria

Trichodesmium erythraeum and *Gloeotrichia* sp. were observed at multiple stations throughout

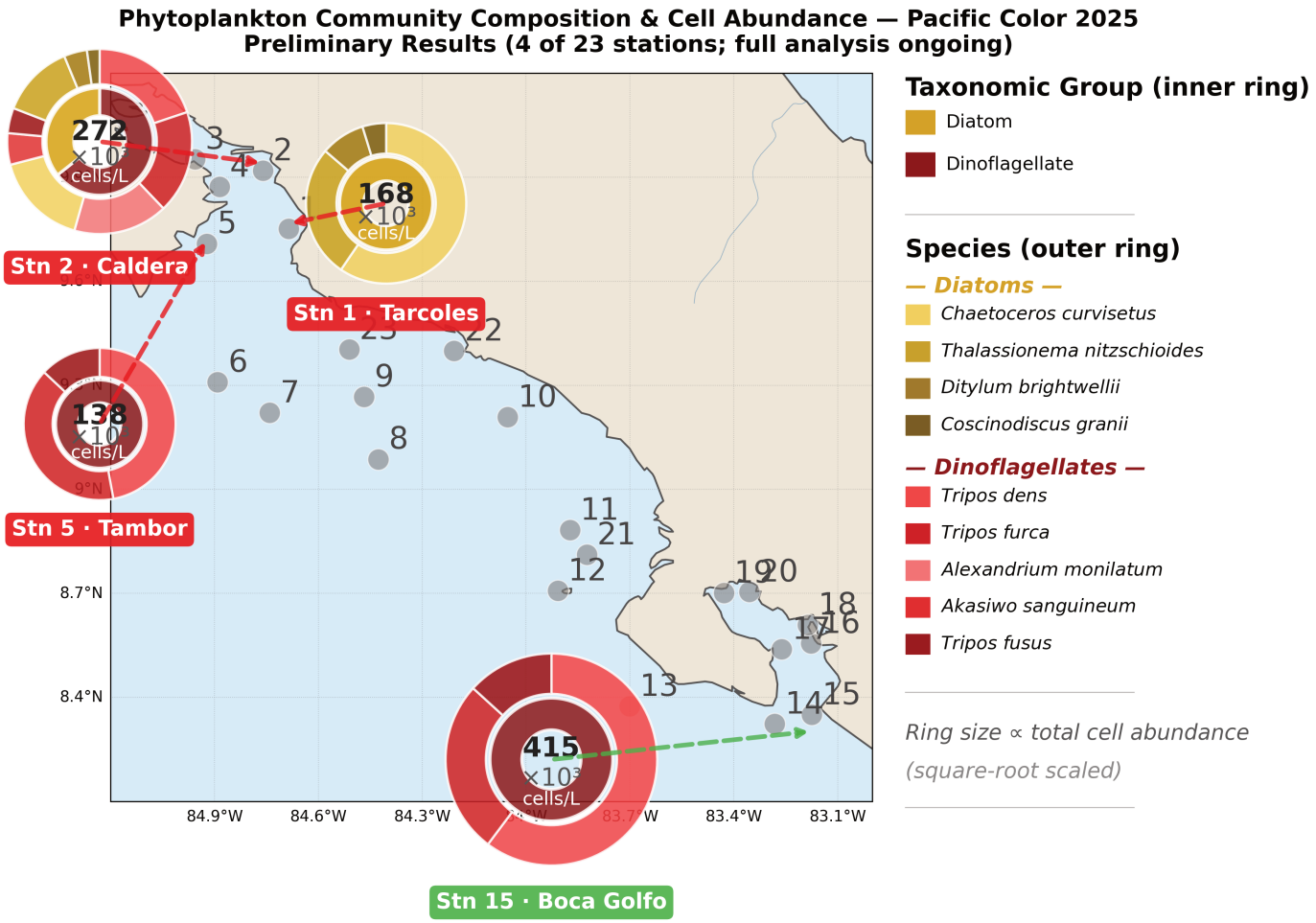


Figure 4.8. Phytoplankton community composition and cell abundance at four stations sampled during the Pacific Color campaign. Ring plots show the relative contribution of individual species (outer ring) and major taxonomic groups (inner ring) to total cell abundance. Ring size is proportional to total cell abundance (square root scaled). Cell counts are expressed in $\times 10^3$ cells L^{-1}. Diatoms are represented in golden-brown tones; dinoflagellates in red tones. All 23 sampling stations are shown as gray dots for spatial context. These results are preliminary; counting and identification are ongoing for the remaining 19 stations. Reported counts represent the most abundant taxa only and should be considered minimum abundance estimates.

the campaign and photographed during light microscopy examination. *Trichodesmium erythraeum* forms characteristic tuft- or puff-shaped colonies and plays a key role in the nitrogen cycle of tropical and subtropical oceans. Quantitative enumeration of cyanobacteria requires sonication of sample aliquots prior to counting to disperse filaments; this step will be performed following completion of all other counts. Cyanobacteria abundance data will be reported in a subsequent version of this report.

4.4.4 Cell Abundance and Taxonomic Composition — Preliminary Results

Preliminary phytoplankton cell counts are available for four of the 23 stations: **Stn. 1**, **Stn. 2**, **Stn. 5**, and **Stn. 15** (Fig. 4.8). Results represent partial counts of the most abundant taxa and should be considered minimum abundance estimates; counting and taxonomic identification are ongoing for the remaining stations.

Total cell abundance varied from 138 × 10^3 cells L^{-1} at **Stn. 5** (Tambor) to 415 × 10^3 cells L^{-1} at **Stn. 15** (Boca Golfo Dulce). *Tripos* spp. emerged as the most ubiquitous and abundant dinoflagellate genus across the four counted stations, notably dominant at **Stn. 5** and **Stn. 15**. *Chaetoceros curvisetus* was the most abundant diatom, recorded at **Stn. 1** and **Stn. 2**. The apparent discrepancy between the high *Tripos*-dominated cell abundance at **Stn. 15** and the low pigment-based microplankton fraction at that station is discussed in Section 4.3.3 and reflects the complementary sensitivities of the two methods rather than an inconsistency in the data.

It must be emphasized that the Pacific Color 2025 campaign represents a single observational snapshot of a coastal system that has been sampled only sporadically. The biogeographic patterns and community structures described here may reflect the particular oceanographic conditions prevailing during this specific February survey as much as they reflect persistent regional structure. Long-term time series from temperate systems have demonstrated that phytoplankton communities are highly dynamic, subject to large interannual variability, episodic regime shifts, and complex patterns of species succession and phenological change governed by physical forcing at multiple temporal and spatial scales; equivalent characterizations remain largely absent for tropical coastal systems such as the Pacific coast of Costa Rica and Central America, where the seasonal cycle, ENSO and other low-frequency climate influences, and the ecological roles of the taxa documented here are still poorly constrained. The present results should therefore be interpreted as a baseline contribution to what must ultimately become a sustained observational effort, rather than a definitive characterization of the regional phytoplankton seascape.

4.5 Fish Larvae and Ichthyoplankton

4.5.1 Larval Fish Diversity and Taxonomic Composition

Fish larvae were collected using 500 µm zooplankton nets deployed during oblique tows at five stations distributed among the Offshore, Coastal, Golfo Dulce, and Coastal Return transects (Stations 8, 9, 13, 19, and 21). Collected fish larvae and fish eggs were separated from the remaining zooplankton samples and subsequently processed at the Centro de Investigación en Estructuras Microscópicas (CIEMIC) and the Zoology Museum of the University of Costa Rica (UCR). High-resolution photographs were obtained for all specimens and independently reviewed by Dr. Beatriz Susana Beltrán León. The taxonomic assignments presented here follow her validated identifications.

A total of 24 larval fish morphotypes representing multiple stages of development were identified from the samples collected during the campaign (Figure 4.9). Of these, 13 morphotypes were identified to species level, six to genus level, four to family level, and one specimen could only be assigned either to the genus *Lutjanus* or to the family Haemulidae. The identified larvae belonged to 15 fish families and represented a broad range of ecological guilds and marine habitats (Table 4.1).

Species identified to species level included *Achirus mazatlanus*, *Monolene asaedai*, *Selar crumenophthalmus*, *Seriola cf. lalandi*, *Polydactylus approximans*, *Sphyraena ensis*, *Mugil cf. cephalus*, *Benthosema panamense*, *Diogenichthys laternatus*, *Halichoeres cf. semicinctus*, *Opistognathus panamensis*, *Prionotus cf. ruscarius*, and *Bathophilus filifer*. Additional larvae were identified at the genus or family level, including representatives of *Symphurus*, *Cynoscion*, *Larimus*, *Scarus*, *Serranus*, Gobiidae, Sciaenidae, Haemulidae, and Lutjanidae.

The larval assemblage reflected the diversity of habitats present along the Pacific coast of Costa Rica. Pelagic and coastal-oceanic species included *Selar crumenophthalmus*, *Seriola cf. lalandi*, *Sphyraena ensis*, and *Mugil cf. cephalus*. Species associated with soft-bottom, demersal, estuarine, and reef habitats included flatfishes (*Achirus maza-*

Table 4.1. Taxonomic identification of fish larvae collected during the Pacific Color 2025 campaign.

Order	Family	Species	Common name
Carangiformes	Achiridae	*Achirus mazatlanus*	Mexican sole
Carangiformes	Bothidae	*Monolene asaedai*	Dark flounder
Carangiformes	Carangidae	*Selar crumenophthalmus*	Bigeye scad
Carangiformes	Carangidae	*Seriola cf. lalandi*	Yellowtail amberjack
Carangiformes	Cynoglossidae	*Symphurus* sp.	Tonguefish
Carangiformes	Polynemidae	*Polydactylus approximans*	Blue bobo
Carangiformes	Sphyraenidae	*Sphyraena ensis*	Mexican barracuda
Eupercaria incertae sedis	Haemulidae	Haemulidae	Grunt
Eupercaria incertae sedis	Lutjanidae	*Lutjanus guttatus* / *L. argentiventris*	Spotted rose snapper / Yellow snapper
Eupercaria incertae sedis	Lutjanidae / Haemulidae	*Lutjanus* sp. / Haemulidae	Snapper / Grunt
Eupercaria incertae sedis	Sciaenidae	*Cynoscion* sp.	Weakfish
Eupercaria incertae sedis	Sciaenidae	*Larimus* sp. 1	Pacific drum
Eupercaria incertae sedis	Sciaenidae	Sciaenidae sp.	Weakfish
Gobiiformes	Gobiidae	Gobiidae sp. 3	True gobies
Gobiiformes	Gobiidae	Gobiidae sp. 4	True gobies
Mugiliformes	Mugilidae	*Mugil cf. cephalus*	Flathead grey mullet
Myctophiformes	Myctophidae	*Benthosema panamense*	Panama lanternfish
Myctophiformes	Myctophidae	*Diogenichthys laternatus*	Diogenes lanternfish
Perciformes	Labridae	*Halichoeres cf. semicinctus*	Rock wrasse
Perciformes	Opistognathidae	*Opistognathus panamensis*	Panamanian jawfish
Perciformes	Scaridae	*Scarus* sp.	Parrotfish
Perciformes	Serranidae	*Serranus* sp. 1	Sea bass
Perciformes	Triglidae	*Prionotus cf. ruscarius*	Searobin
Stomiiformes	Stomiidae	*Bathophilus filifer*	Slender dragonfish

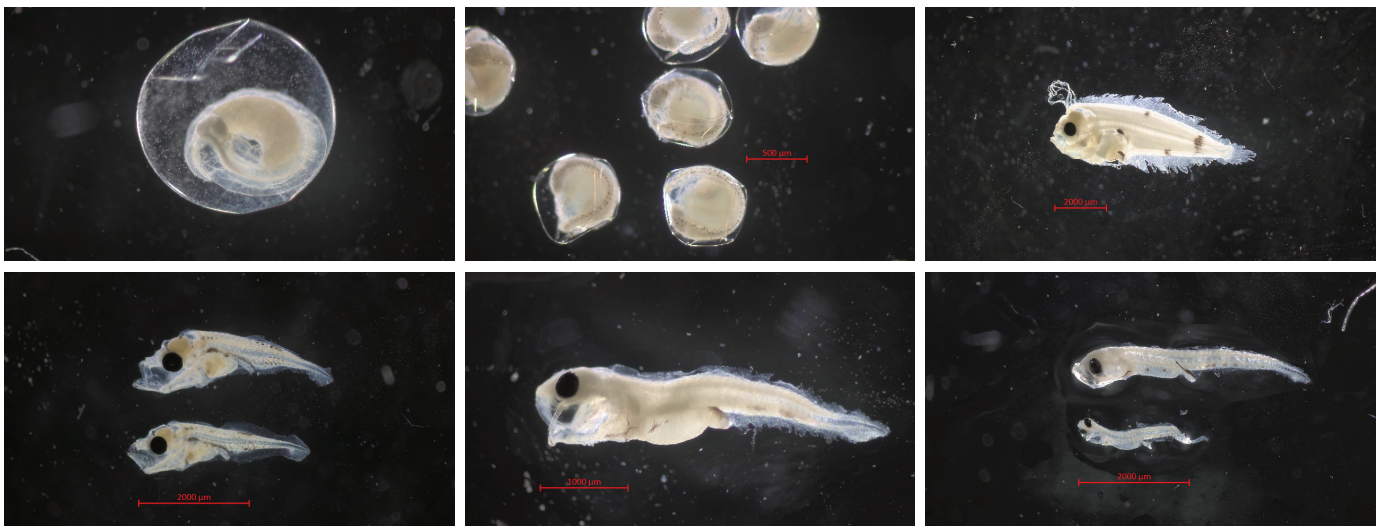


Figure 4.9. Representative ichthyoplankton specimens collected during the Pacific Color 2025 campaign. (A–B) Unidentified fish eggs at different magnifications; (C) *Symphurus* sp.; (D) *Selar crumenophthalmus*; (E) *Benthosema panamense*; (F) *Diogenichthys laternatus*. Photographs were obtained during taxonomic processing at CIEMIC and subsequently verified by Dr. Beatriz Susana Beltrán León.

-tlanus, *Monolene asaedai*, *Symphurus* spp.), snappers (Lutjanidae), grunts (Haemulidae), weakfishes (Sciaenidae), gobies (Gobiidae), wrasses (*Halichoeres*), jawfishes (*Opistognathus*), parrotfishes (*Scarus*), sea basses (*Serranus*), and sea robins (*Prionotus*). Mesopelagic taxa were also present, including the lanternfishes *Benthosema panamense* and *Diogenichthys laternatus*, as well as the dragonfish *Bathophilus filifer*.

The identification of 24 larval morphotypes from only five sampling stations highlights the considerable diversity of larval fishes present within the study region. The assemblage included coastal, estuarine, reef-associated, pelagic, and mesopelagic taxa, demonstrating the strong ecological connectivity between nearshore and oceanic environments along the Pacific coast of Costa Rica. These results provide a valuable baseline for future studies examining the spatial and temporal variability of ichthyoplankton communities in the region.

4.5.2 Collection Status and Future Work

Fish egg specimens and the remaining zooplankton community have not yet been fully identified to the lowest possible taxonomic level. Additional processing and taxonomic verification are currently underway. All processed ichthyoplankton material will be cataloged, curated, and incorporated into the ichthyoplankton collection of the Zoology Museum of the University of Costa Rica, where it will remain available for future taxonomic, ecological, and biodiversity studies.

4.5.3 PACE Satellite Data Acquisition and Spatial Coverage

To support the optical validation objectives of the Pacific Color 2025 campaign, Level-2 Ocean Color Instrument (OCI) data from the PACE satellite were acquired. Data retrieval focused on overpasses that coincided spatially with the study area and temporally within a ±24-hour window of the *in situ* sampling operations and continuous DALEC radiometric measurements.

A total of 9 PACE granules were identified and downloaded (Table 4.2). The spatial extent of these satellite footprints in relation to the cruise track and discrete sampling stations is illustrated in Fig. 4.10. By mapping the outer boundaries of each PACE granule, it was confirmed that these specific overpasses provided the necessary spatial overlap to attempt radiometric matchups with the shipboard data.

Table 4.2. PACE OCI Level-2 AOP granules evaluated for radiometric matchups during the Pacific Color 2025 campaign. Dates and times are in GMT.

Date	Time	Generic Granule Prefix
2025-02-16	19:02:09	PACE_OCI.20250216T190209
2025-02-17	17:59:23	PACE_OCI.20250217T175923
2025-02-17	18:04:23	PACE_OCI.20250217T180423
2025-02-18	18:34:57	PACE_OCI.20250218T183457
2025-02-19	19:10:31	PACE_OCI.20250219T191031
2025-02-20	18:07:43	PACE_OCI.20250220T180743
2025-02-21	18:43:17	PACE_OCI.20250221T184317
2025-02-22	17:40:29	PACE_OCI.20250222T174029
2025-02-22	19:18:51	PACE_OCI.20250222T191851

4.5.4 Preliminary DALEC and PACE Radiometry Matchups

To evaluate the preliminary performance of PACE OCI in the study area, *in situ* remote sensing reflectance (R_{rs}) measured continuously by the DALEC sensor was matched with Level-2 PACE overpasses. Validating satellite data in tropical coastal regions is notoriously challenging due to persistent cloud cover, sunglint, and the optical complexity of nearshore waters.

Rather than limiting matchups to discrete sampling stations, a continuous-track matchup approach was used to maximize the retrieval of candidate satellite observations. Individual DALEC measurements were associated with nearby PACE OCI Level-2 observations using an expanded temporal search window of ±24 hours and spatial extraction based on a 3×3 macropixel window centered on the nearest available satellite pixel.

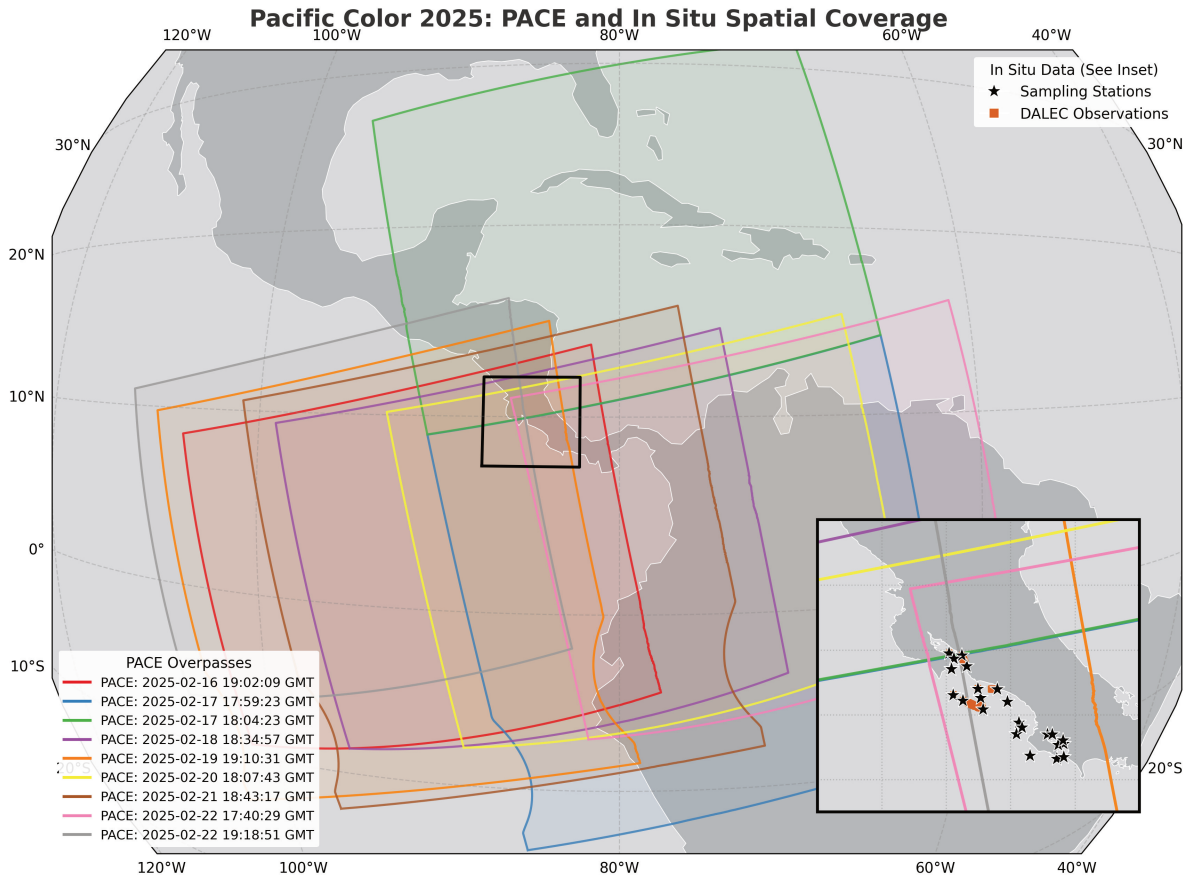


Figure 4.10. Spatial coverage of the 9 PACE OCI Level-2 AOP granules (colored polygons) relative to the *in situ* sampling stations (stars) and continuous DALEC observations (squares) during the Pacific Color 2025 campaign.

A total of 63 candidate PACE–DALEC matchups were identified across 20 sampling stations distributed among five survey transects. For each candidate, temporal separation (Δt), spatial offset, Level-2 quality flags, and spectral agreement metrics were evaluated when sufficient valid radiometric information was available. This approach was designed to characterize the full range of potential matchups rather than restricting the analysis to only unflagged satellite observations.

The results confirmed that radiometric validation in tropical coastal environments remains particularly challenging. Although numerous candidate satellite observations were identified within the prescribed spatial and temporal windows, the majority were affected by one or more standard NASA Level-2 quality flags associated with cloud contamination, land contamination, viewing geometry, or atmospheric correction uncertainty. The frequency of Level-2 quality flags encountered among candidate matchups is summarized in Table 4.3. Cloud contamination (`CLDICE`) was by far the most common limitation, followed by large satellite zenith angles (`HISATZEN`) and coastal adjacency effects (`COASTZ`). Warning flags associated with product quality (`PRODWARN`), stray light contamination (`STRAYLIGHT`), and atmospheric correction uncertainty (`ATMWARN`) were also encountered, whereas explicit land contamination (`LAND`) was comparatively uncommon.

Despite the large number of candidate observations, only 10 candidate matchups produced

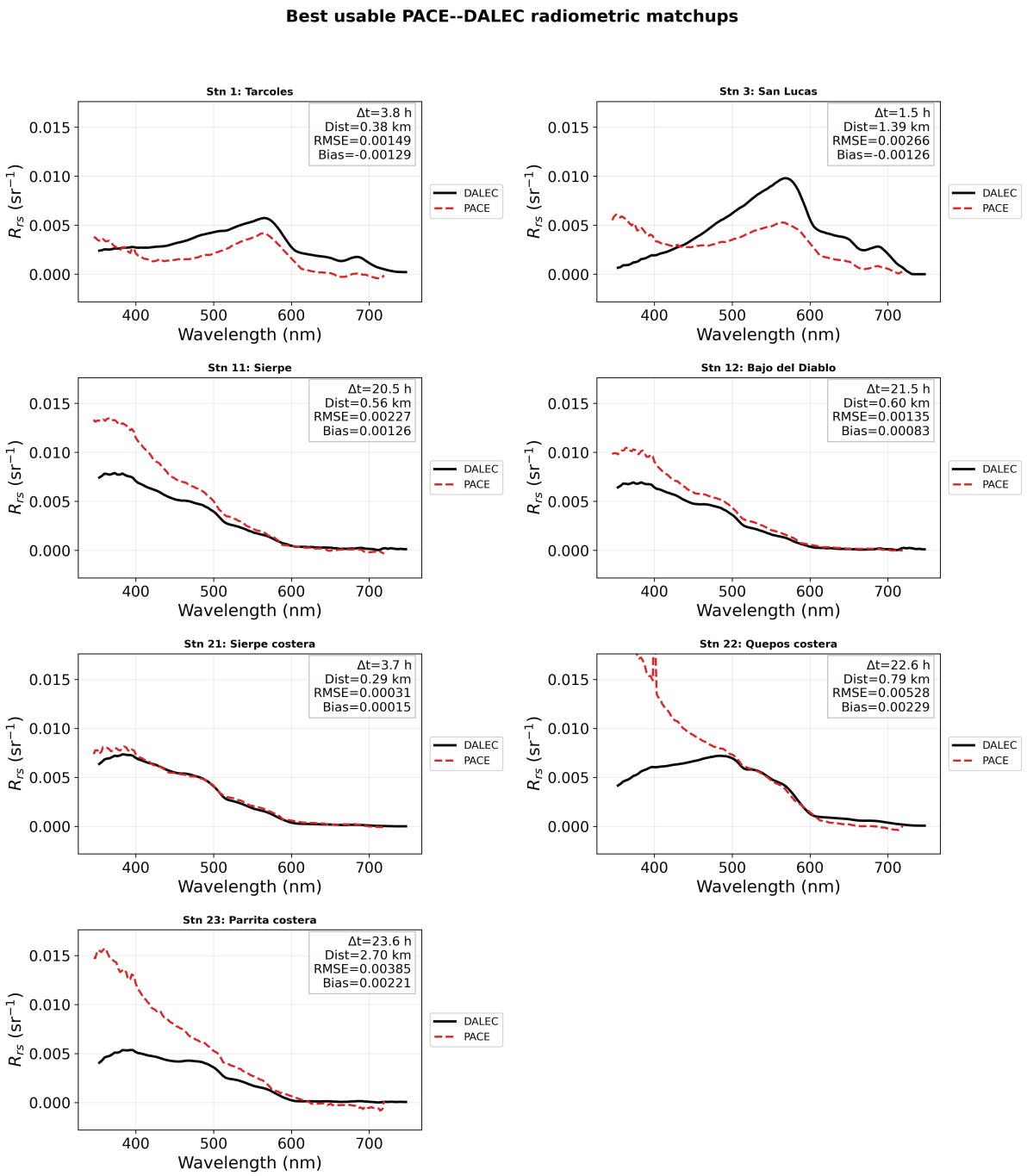


Figure 4.11. Selected PACE–DALEC candidate matchups retained for further evaluation. Spectral comparisons between *in situ* DALEC remote sensing reflectance (R_{rs}; solid black lines) and the corresponding PACE OCI Level-2 retrievals (dashed red lines) for the seven candidate matchups identified as the most suitable for quantitative evaluation. Candidates were selected from the complete matchup inventory by requiring computable spectral comparison metrics and excluding observations affected by explicit `LAND` or `CLDICE` quality flags. Each panel reports the temporal separation (Δt), spatial offset, Root Mean Square Error (RMSE), and Mean Bias between the satellite and *in situ* spectra.

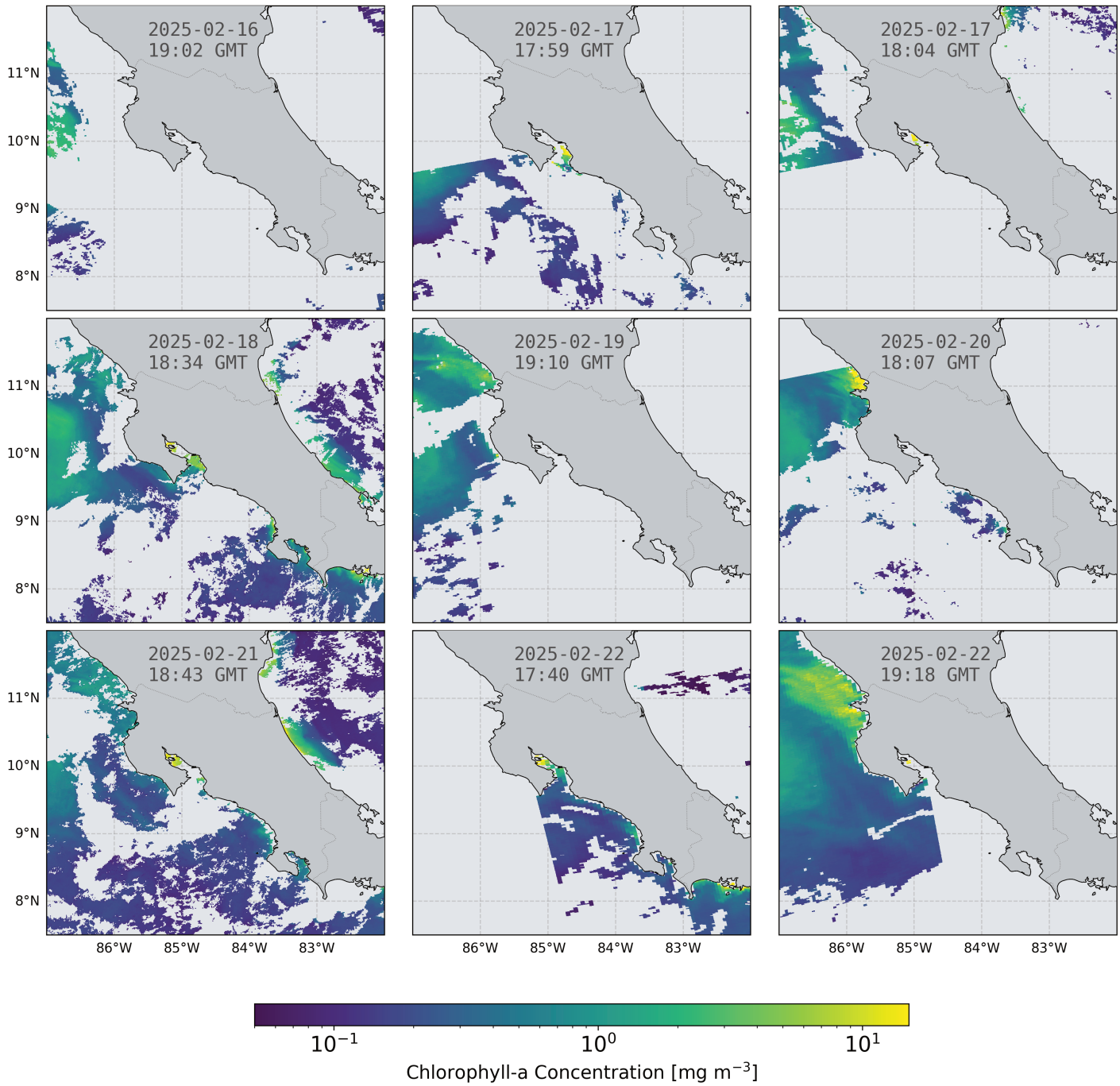


Figure 4.12. Preliminary PACE OCI Level-2 chlorophyll *a* (mg m^{-3}) spatial coverage over the Pacific Color 2025 study area. The nine panels represent the individual overpasses acquired between February 16 and February 22, 2025. Data are plotted on a unified logarithmic scale (Log_{10}). Gray areas over the ocean denote pixels masked by standard quality flags, predominantly due to the anomalously high cloud cover experienced during the campaign. Valid data retrieval was severely limited, directly impacting the availability of pristine radiometric matchups.

Table 4.3. Frequency of PACE Level-2 flags among evaluated candidate matchups. Counts are shown for all candidate rows and for the closest-candidate-per-station table.

Flag	All candidates	Closest per station
CLDICE	51	24
HISATZEN	17	8
COASTZ	11	3
PRODWARN	6	3
STRAYLIGHT	6	2
LAND	4	1
ATMWARN	3	1
NONE	2	0

computable spectral comparison metrics, representing seven unique stations. The spectral agreement for these retained candidates is shown in Fig. 4.11. Matchups affected by explicit LAND or CLDICE flags were generally unsuitable for quantitative validation because no reliable water-leaving radiometric signal could be retrieved. Consequently, only a small subset of candidate observations could be considered potentially useful for further evaluation.

The prevalence of cloud-related and geometric quality flags indicates that data availability, rather than spatial proximity to the shipboard observations, was the primary limitation during the campaign. Persistent cloud cover substantially reduced the number of valid Level-2 retrievals, while coastal adjacency effects and challenging viewing conditions further limited the availability of usable pixels in nearshore waters.

Overall, the analysis demonstrates that the principal challenge was not the identification of nearby satellite observations, but rather the availability of sufficiently high-quality Level-2 retrievals suitable for quantitative validation. While numerous candidate matchups were identified, only a small fraction met the criteria necessary for meaningful radiometric comparison. All retained candidates were free of explicit LAND and CLDICE flags, although several still carried warning flags such as PRODWARN, COASTZ, STRAYLIGHT, ATMWARN, or HISATZEN. These findings emphasize the continued importance of dedicated *in situ* radiometric measurements for validating and improving satellite ocean-color products in optically complex tropical coastal waters.

4.5.5 Spatial Distribution of Satellite Retrievals and Environmental Constraints

To assess the spatial availability of OCI data during the study period, the Level-2 biogeochemical (BGC) products, specifically the chlorophyll-*a* concentration (chlor_a), were evaluated across the 9 acquired PACE overpasses (Fig 4.12).

A visual inspection of the spatial coverage reveals a critically low retrieval rate across the study area for the duration of the campaign. Despite the Pacific Color 2025 cruise taking place during the boreal winter (February), which historically corresponds to the regional dry season characterized by clear skies and strong trade winds (e.g., the Papagayo wind jet), the meteorological conditions encountered were anomalously cloudy and unseasonably rainy.

Consequently, the standard atmospheric correction and quality-control masking algorithms (primarily the cloud/ice CLDICE flag) discarded the vast majority of the marine pixels within the Gulf of Nicoya and the adjacent coastal waters. Valid chlorophyll-*a* retrievals were largely restricted to sparse, fragmented patches in the offshore regions or narrow, transient gaps in the cloud cover.

This pronounced lack of contiguous, clear-sky spatial coverage fundamentally constrained the optical validation efforts. The anomalous cloud fraction directly explains the paucity of high-quality satellite–*in situ* matchups discussed previously, as the probability of a clear satellite pixel spatially aligning with a shipboard radiometric measurement during the exact time of the overpass was exceptionally low.

4.5.6 Level-3 Chlorophyll a Composites and HPLC Matchups

To further assess the availability of valid satellite retrievals and compensate for daily cloud masking, a 7-day composite (Level-3 mapped 4 km pixel, L3m) of PACE OCI TChl *a* was generated for the

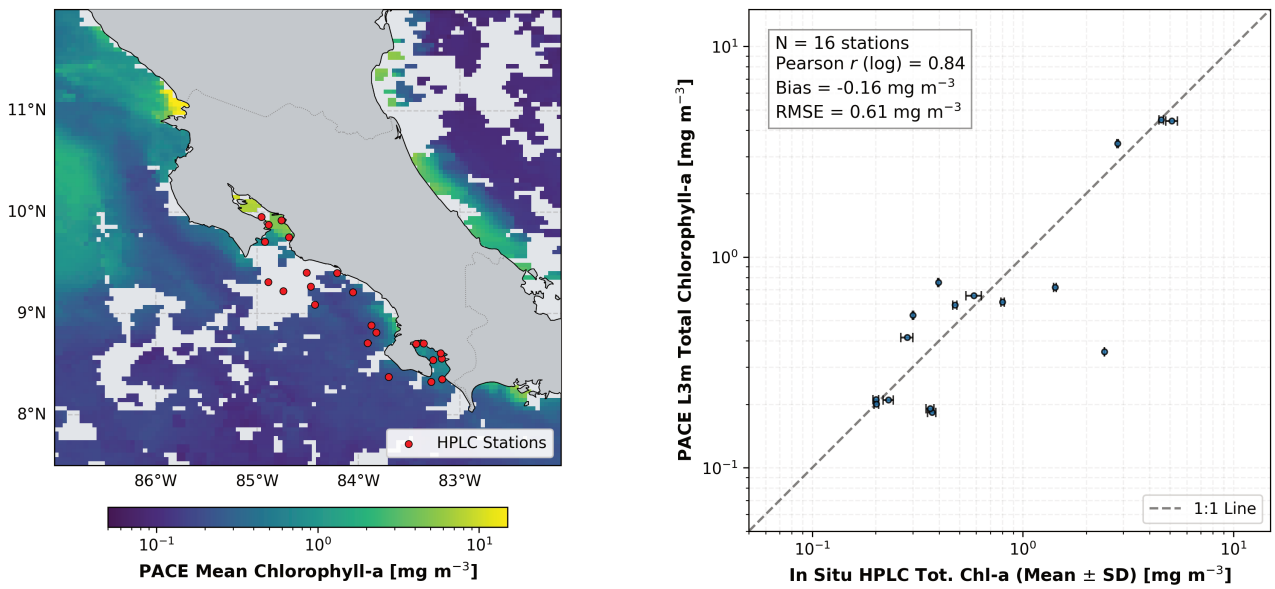


Figure 4.13. Preliminary PACE OCI Level-3 Chlorophyll *a* and HPLC matchups. (Left) A 7-day composite of PACE OCI chlorophyll *a* concentration (mg m^{-3}) for the cruise period, with red circles indicating the locations of *in situ* HPLC surface stations. Note the prominent data gap in the central coastal and offshore transect region due to persistent cloud cover. (Right) Scatter plot comparing the *in situ* HPLC total chlorophyll *a* means against the corresponding PACE L3m pixel retrievals for the 16 successfully matched stations. Horizontal error bars denote the standard deviation of the *in situ* replicates. The dashed line represents the 1:1 agreement line.

duration of the cruise ± 1 day (February 16–22, 2025; Fig 4.13). While temporal aggregation typically mitigates the impact of transient cloud cover, the resulting composite reinforces the severity of data loss during this anomalously cloudy period. Although valid satellite pixels were successfully aggregated across the broader offshore Pacific region and within the Gulf of Nicoya, a considerable data gap persists exactly over the region where the primary coastal and offshore transects were conducted.

Despite these severe spatial limitations, preliminary matchups were evaluated between the PACE L3m composite and *in situ* TChl *a* (`Tot_Chl_a`) measured analytically via HPLC from surface samples (≤ 5 m depth). Replicate measurements at each station were averaged to compute *in situ* mean and standard deviations.

A total of 16 *in situ* stations successfully matched with valid L3m satellite pixels. Statistical evaluation of these matchups yielded a strong positive correlation, with a Pearson coefficient of $r = 0.84$ ($\log_{10}$-transformed). However, the satellite retrievals exhibited a slight overall underestimation relative to the HPLC measurements, reflected by a Mean Bias of -0.16 mg m^{-3} and a Root Mean Square Error (RMSE) of 0.61 mg m^{-3} (Fig 4.13). These preliminary results indicate encouraging agreement between PACE OCI Level-3 chlorophyll retrievals and *in situ* HPLC measurements, notwithstanding the temporal smoothing inherent to the 7-day composite.

4.5.7 AVUELO / AVIRIS-3 Airborne Observations

During the Pacific Color 2025 campaign, the NASA AVUELO airborne mission conducted multiple flights using the AVIRIS-3 (Airborne Visible/Infrared Imaging Spectrometer) instrument over the Costa Rican Pacific coast. To evaluate the potential for combined airborne and ship-based

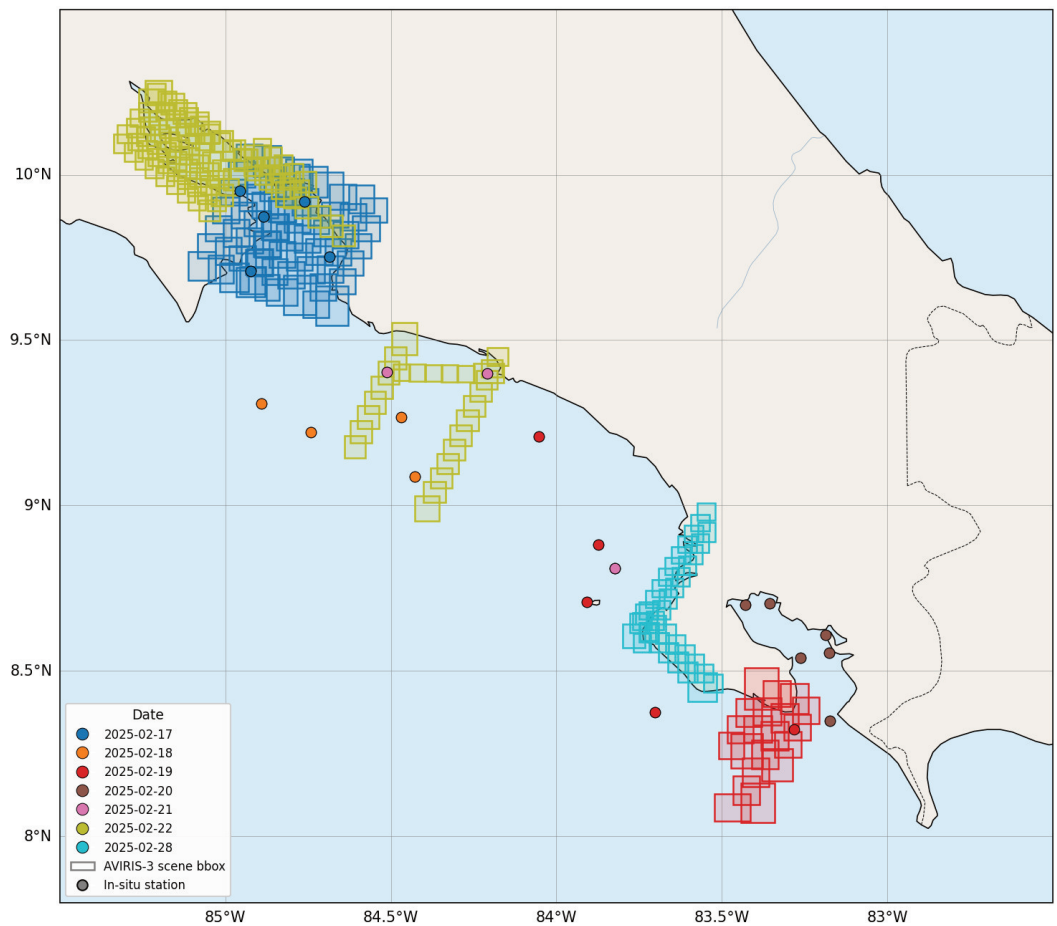


Figure 4.14. Spatial and temporal overlap between AVUELO/AVIRIS-3 flight granules and Pacific Color 2025 *in situ* sampling stations. The bounding edges of the airborne scenes and the *in situ* station markers are both color-coded by date to illustrate temporal alignment alongside spatial coverage. Note the strong spatio-temporal coincidence on February 17 during the Gulf of Nicoya sampling, as well as the overlap with at least one station sampled on February 19.

analyses, flight granules were assessed for both spatial and temporal overlap with the Pacific Color *in situ* sampling stations.

There were multiple days where AVUELO flight paths successfully targeted areas encompassing our study region (Fig 4.14). The most significant coordination occurred on February 17, which demonstrated very close spatial and temporal alignment between the AVUELO overflights and our ship-based sampling operations within the Gulf of Nicoya. Additionally, there was spatial overlap for at least one *in situ* station during the sampling operations on February 19, where the vessel's position intersected the airborne flight path for that day.

These temporally and spatially coincident datasets will be highly valuable for future post-cruise validation and scaling of the *in situ* optical and biogeochemical measurements.

Acknowledgments

The Pacific Color 2025 campaign was funded in part by the U.S. National Aeronautics and Space Administration (NASA) PACE Early Adopter Program. The authors gratefully acknowledge the support of NASA's Goddard Space Flight Center (GSFC) Ocean Ecology Laboratory, whose Field Support Group provided HPLC pigment analysis

through their centralized quality-assured facility. Phytoplankton pigment samples were analyzed by Crystal Thomas (NASA GSFC/SSAI).

Instrumental and logistical support was generously provided by colleagues at the University of South Florida (USF) College of Marine Science: Chuanmin Hu, Brian Barnes, and Jennifer Cannizzaro (Optical Oceanography Laboratory) contributed optical instrumentation and expertise, and Kendra Daly (Zooplankton Ecology Laboratory) and Mark Luther provided additional equipment that was essential to the success of the field campaign. The Universidad Nacional de Costa Rica (UNA) and the Universidad de Costa Rica (UCR) contributed research equipment and scientific expertise that were integral to the execution of the sampling program and the preliminary analyses presented in this report.

Shore-based logistical support was provided by Safe Harbor Los Sueños Marina (Herradura), Marina Pez Vela (Quepos), and Crocodile Bay Resort and Botanika (Puerto Jiménez), whose assistance with vessel operations, fueling, and coordination greatly facilitated sampling across the study area. The authors extend their sincere gratitude to the captain and crew of the sportfishing yacht *Amejaye* for their professionalism, seamanship, and commitment throughout the cruise, without whom the successful completion of the sampling program would not have been possible.

Bibliography

Acuña Piedra, J. F. and Quesada-Román, A. (2017). Cambios en el uso y cobertura de la tierra entre 1948 y 2012 en el Humedal Nacional Térraba-Sierpe, Costa Rica. *Revista de Ciencias Marinas y Costeras*, 9(2):9–28.

Amador, J. A., Alfaro, E. J., Lizano, O. G., and Magaña, V. O. (2006). Atmospheric forcing of the eastern tropical Pacific: A review. *Progress in Oceanography*, 69:101–142.

American Public Health Association, American Water Works Association, and Water Environment Federation (1999). *Standard Methods for the Examination of Water and Wastewater*. American Public Health Association, Washington, DC.

Aurin, D. A., Vandenberg, N., Gossn, J. I., Ramsay, A., Haentjens, N., Bialek, A., Deru, A., Gu, H., Abdelmegid, M., Mabit, R., Costa, M., Bretagnon, M., and Bai, G. (2024). HyperInSPACE Community Processor (HyperCP): Hyperspectral Data Processing Software for Ocean Color.

Bailey, S. W. and Werdell, P. J. (2006). A multi-sensor approach for the on-orbit validation of ocean color satellite data products. *Remote Sensing of Environment*, 102:12–23.

Balla, A., Teofilović, V., and Kiss, T. (2024). Microplastic contamination of fine-grained sediments and its environmental driving factors along a lowland river: Three-year monitoring of the Tisza River in Central Europe. *Hydrology*, 11(1):11.

Balzano, S., Abs, E., and Leterme, S. C. (2015). Protist diversity along a salinity gradient in a coastal lagoon. *Aquatic Microbial Ecology*, 74:263–277.

Brando, V., Lovell, J., King, E., Boadle, D., Scott, R., and Schroeder, T. (2016). The potential of autonomous ship-borne hyperspectral radiometers for the validation of ocean color radiometry data. *Remote Sensing*, 8(2):150.

Brenes, C. L. (1985). Condiciones de movimiento geostrófico para la corriente costera de Costa Rica. *Uniciencia*, 2(1):21–27.

Brenes, C. L., Coen, J. E., Chelton, D. B., Enfield, D. B., Leon, S., and Ballestero, D. (2003). Wind driven upwelling in the Gulf of Nicoya, Costa Rica. *International Journal of Remote Sensing*, 24(5):1127–1133.

Brenes, C. L., Lavín, M. F., and Mascarenhas, A. (2008). Geostrophic circulation between the Costa Rica Dome and Central America. *Deep-Sea Research Part I*, 55(5):608–629.

Brodrick, P. G., Chlus, A. M., Eckert, R., Chapman, J. W., Eastwood, M., Geier, S., Lundeen, S. R., Olson-Duvall, W., Rios, L. M., Jensen, D. J., Bernas, M., Thompson, D. R., and Green, R. O. (2025). AVUELO AVIRIS-3 orthocorrected surface reflectance (provisional calibration), version 1. Accessed: 2026-04-15.

Broenkow, W. W. (1964). The distribution of nutrients in the Costa Rica Dome in the eastern tropical Pacific Ocean. *Limnology and Oceanography*, 10:40–52.

Brugnoli-Olivera, E. and Morales-Ramírez, A. (2008). Trophic planktonic dynamics in a tropical estuary, Gulf of Nicoya, Pacific coast of Costa Rica during El Niño 1997 event. *Revista de Biología Marina y Oceanografía*, 43(1):75–89.

Chaves, J. E. (1997). A preliminary assessment of the annual mass balance of nitrogen and phosphorus in the Gulf of Nicoya, Costa Rica. Master's thesis, University of Rhode Island, Kingston, RI.

Claustre, H. (1994). The trophic status of various oceanic provinces as revealed by phytoplankton pigment signatures. *Limnology and Oceanography*, 39(5):1206–1210.

Cortés, J. (2016). The Pacific coastal and marine ecosystems. In Kappelle, M., editor, *Costa Rican Ecosystems*, chapter 5. University of Chicago Press, Chicago, IL.

Dalsgaard, T., Canfield, D. E., Petersen, J., Thamdrup, B., and Acuña-González, J. (2003). N_2 production by the anammox reaction in the anoxic water column of Golfo Dulce, Costa Rica. *Nature*, 422:606–608.

Epifanio, C. E., Maurer, D., and Dittel, A. I. (1983). Seasonal changes in nutrients and dissolved oxygen in the Gulf of Nicoya, a tropical estuary. *Hydrobiologia*, 101:231–238.

Fiedler, P. C. (2002). The annual cycle and biological effects of the Costa Rica Dome. *Deep-Sea Research Part I*, 49:321–338.

Fiedler, P. C. and Lavín, M. F. (2016). Oceanographic conditions of the eastern tropical Pacific. In Glynn, P. W., Manzello, D. P., and Enochs, I. C., editors, *Coral Reefs of the Eastern Tropical Pacific*, volume 8 of *Coral Reefs of the World*, pages 59–83. Springer, Dordrecht.

Fiedler, P. C., Redfern, J. V., and Ballance, L. T. (2017). Oceanography and cetaceans of the Costa Rica Dome region. Technical Report NOAA-TM-NMFS-SWFSC-590, NOAA, National Marine Fisheries Service, Southwest Fisheries Science Center, La Jolla, CA.

Fiedler, P. C. and Talley, L. D. (2006). Hydrography of the eastern tropical Pacific: A review. *Progress in Oceanography*, 69(2):143–180.

Gocke, K., Cortés, J., and Villalobos, C. (1990). Effects of red tides on oxygen concentration and distribution in the Golfo de Nicoya, Costa Rica. *Revista de Biología Tropical*, 38(2B):401–407.

Green, R. O., Schaepman, M. E., Mouroulis, P., Geier, S., Shaw, L., Hueini, A., Bernas, M., McKinley, I., Smith, C., Wehbe, R., Eastwood, M., Vinckier, Q., Liggett, E., Zandbergen, S., Thompson, D., Sullivan, P., Sarture, C., Van Gorp, B., and Helmlinger, M. (2022). Airborne visible/infrared imaging spectrometer 3 (AVIRIS-3). In *2022 IEEE Aerospace Conference (AERO)*.

Hansen, H. P. and Koroleff, F. (2007). Determination of nutrients. In Grasshoff, K., Kremling, K., and Ehrhardt, M., editors, *Methods of Seawater Analysis*, pages 159–228. Wiley-VCH, Weinheim, 3 edition.

Hargraves, P. E. and Víquez M., R. (1985). Spatial and temporal distribution of phytoplankton in the Gulf of Nicoya, Costa Rica. *Bulletin of Marine Science*, 37(2):577–585.

Hasan, A. B., Reza, A. S., Siddique, M. A. B., Akbor, M. A., Nahar, A., Hasan, M., and Moniruzzaman, M. (2023). Spatial distribution, water quality, human health risk assessment, and origin of heavy metals in groundwater and seawater around the ship-breaking area of bangladesh. *Environmental Science and Pollution Research*, 30(6):16210–16235.

Hebbeln, D. and Cortés, J. (2001). Sedimentación en el Golfo Dulce, Costa Rica. *Revista de Biología Tropical*, 49(Suppl. 2):93–94.

Hooker, S. B. et al. (2002). The Second SeaWiFS HPLC analysis round-robin Experiment (SeaHARRE-2). Technical Report NASA/TM-2002-211606, NASA Goddard Space Flight Center, Greenbelt, MD.

Kessler, W. S. (2006). The circulation of the eastern tropical Pacific: A review. *Progress in Oceanography*, 69(2):181–217.

Kress, N., Leon Coto, S., Brenes, C. L., Brenner, S., and Arroyo, G. (2002). Horizontal transport and seasonal distribution of nutrients, dissolved oxygen and chlorophyll *a* in the Gulf of Nicoya, Costa Rica: A tropical estuary. *Continental Shelf Research*, 22:51–66.

Liu, N., Yang, Y., Li, F., Ge, F., and Kuang, Y. (2016). Importance of controlling pH-dependent dissolved inorganic carbon to prevent algal bloom outbreaks. *Bioresource Technology*, 220:246–253.

Lizano, O. G. (2015). La dinámica oceanográfica frente al Humedal Nacional Térraba-Sierpe y su relación con la muerte del manglar. *Revista de Biología Tropical*, 63(Suppl. 1):29–46.

Lizano, O. G., Amador, J. A., and Soto, R. (2001). Caracterización de manglares de Centroamérica con sensores remotos. *Revista de Biología Tropical*, 49(Supl. 2):331–340.

Massana, R., Murray, A. E., Preston, C. M., and DeLong, E. F. (1997). Vertical distribution and phylogenetic characterization of marine planktonic archaea in the santa barbara channel. *Applied and Environmental Microbiology*, 63(1):50–56.

Mobley, C. D. (1999). Estimation of the remote-sensing reflectance from above-surface measurements. *Applied Optics*, 38:7442–7455.

Mobley, C. D. (2015). Polarized reflectance and transmittance properties of windblown sea surfaces. *Applied Optics*, 54:4828–4849.

Morales-Ramírez, A. (2011). La diversidad marina del Golfo Dulce, Pacífico sur de Costa Rica: Amenazas a su conservación. *Biocenosis*, 24(1–2).

Palter, J., Leon Coto, S., and Ballestero, D. (2007). The distribution of nutrients, dissolved oxygen and chlorophyll *a* in the upper Gulf of Nicoya, Costa Rica, a tropical estuary. *Revista de Biología Tropical*, 55(2):427–436.

Parada, A. E., Needham, D. M., and Fuhrman, J. A. (2016). Every base matters: Assessing small subunit rrna primers for marine microbiomes with mock communities, time series and global field samples. *Environmental Microbiology*, 18(5):1403–1414.

Prosser, K. N., Valenti, T. W., Hayden, N. J., Neisch, M. T., Hewitt, N. C., Umphres, G. D., Gable, G. M., Grover, J. P., Roelke, D. L., and Brooks, B. W. (2012). Low pH preempts bloom development of a toxic haptophyte. *Harmful Algae*, 20:156–164.

Quesada-Alpízar, M. A. and Morales-Ramírez, A. (2004). Comportamiento de las masas de agua en el Golfo Dulce, Pacífico de Costa Rica: Período 1999–2000. *Revista de Biología Tropical*, 52(Suppl. 2):95–106.

Shetty, A. and Goyal, A. (2022). Total organic carbon analysis in water: A review of current methods. *Materials Today: Proceedings*, 65:3881–3886.

Svendsen, H., Rosland, R., Myking, S., Vargas, J. A., Lizano, O. G., and Alfaro, E. J. (2006). A physical-oceanographic study of Golfo Dulce, Costa Rica. *Revista de Biología Tropical*, 54(Suppl. 1):147–170.

Uitz, J., Claustre, H., Morel, A., and Hooker, S. B. (2006). Vertical distribution of phytoplankton communities in open ocean: An assessment based on surface chlorophyll. *Journal of Geophysical Research*, 111.

Van Heukelem, L. and Thomas, C. S. (2001). Computer-assisted high-performance liquid chromatography method development with applications to the isolation and analysis of phytoplankton pigments. *Journal of Chromatography A*, 910:31–49.

Vargas, J. A. (1995). The Gulf of Nicoya estuary, Costa Rica: Past, present, and future cooperative research. *Helgoländer Meeresuntersuchungen*, 49:821–828.

Vargas, J. A. (2016). The Gulf of Nicoya estuarine ecosystem. In Kappelle, M., editor, *Costa Rican Ecosystems*, pages 139–161. University of Chicago Press, Chicago, IL.

Vidussi, F., Claustre, H., Manca, B. B., Luchetta, A., and Marty, J. C. (2001). Phytoplankton pigment distribution in relation to upper thermocline circulation in the eastern Mediterranean Sea during winter. *Journal of Geophysical Research*, 106:19939–19956.

Wei, S., Zhuang, G., Cheng, L., Zhao, T., and Wang, H. (2022). The proliferation rule of *Microcystis aeruginosa* under different initial pH conditions and its influence on the pH value of the environment. *Environmental Science and Pollution Research*, 29:13835–13844.

Werdell, P. J. and Bailey, S. W. (2005). An improved *in situ* bio-optical data set for ocean color algorithm development and satellite data product validation. *Remote Sensing of Environment*, 98:122–140.

Wolff, M. and Vargas, J. A. (1994). RV Victor Hensen Costa Rica Expedition 1993/1994. Cruise Report. Cruise Report, Center for Tropical Marine Ecology (ZMT), Bremen, Germany.

Wyrtki, K. (1964). Upwelling in the Costa Rica Dome. *Fishery Bulletin*, 63:355–372.

Zibordi, G. et al. (2004). Comparison of above-water and in-water optical measurements in the Adriatic Sea. *IEEE Transactions on Geoscience and Remote Sensing*, 42:671–682.

Zibordi, G. et al. (2015). AERONET-OC: An assessment of above water radiometry for ocean color satellite validation. *IEEE Transactions on Geoscience and Remote Sensing*, 53:4194–4209.

A. Appendix

A.1 Data Management Notes

The Pacific Color 2025 campaign is committed to the principles of Open Science and adheres to the FAIR (Findable, Accessible, Interoperable, and Reusable) data practices. To maximize the scientific return on investment and ensure transparency, all data collected during this expedition will be preserved, cataloged, and made publicly accessible through designated long-term repositories following stringent quality assurance and quality control (QA/QC) procedures.

A.1.1 Data Repositories and Formatting

To guarantee interoperability and discoverability, datasets will be distributed across appropriate discipline-specific repositories:

- **Marine Optical and Biogeochemical Data:** All *in situ* radiometric measurements (e.g., DALEC), inherent optical properties (IOPs), and biogeochemical data (e.g., HPLC pigments, nutrients) will be submitted to the NASA SeaWiFS Bio-optical Archive and Storage System (SeaBASS). Prior to submission, all files will be strictly formatted to adhere to SeaBASS metadata header requirements and standard variable naming conventions to facilitate direct integration into the PACE validation data stream.
- **Airborne Hyperspectral Data:** The AVUELO AVIRIS-3 orthocorrected surface reflectance datasets, acquired in coordination with this cruise, are cataloged and hosted by the Oak Ridge National Laboratory Distributed Active Archive Center (ORNL DAAC) and are discoverable via NASA's Earthdata portal.
- **Genomic Data:** Raw sequence reads and assembled amplicons for the prokaryotic (16S rRNA) and eukaryotic (18S rRNA) community structures will be deposited into the National Center for Biotechnology Information (NCBI) Sequence Read Archive (SRA) or an equivalent public genetic sequence database, accompanied by rigorous environmental metadata (MIxS standards).

A.1.2 Discoverability and DOI

Upon successful ingestion into their respective repositories, permanent Digital Object Identifiers (DOIs) will be procured for each dataset. Comprehensive metadata records, including spatiotemporal bounds, instrument calibration histories, and processing methodologies, will be linked to these DOIs to ensure full discoverability across global data catalogs.

A.1.3 Data Usage, Embargo, and Citation

The Pacific Color 2025 Science Team supports rapid data dissemination. While raw and preliminary data may be shared among immediate collaborators during the initial analysis phase, the finalized Level-2/Level-3 *in situ* datasets will be made publicly available once post-cruise calibrations and final QA/QC protocols are complete.

Users of these datasets are expected to adhere to standard scientific ethics regarding data usage:

1. **Citation:** Any publication, presentation, or product derived from these data must properly cite the specific dataset DOIs as well as this official cruise report.
2. **Acknowledgment:** Users are requested to acknowledge the collaborative funding and logistical support provided by NASA, the Federación Costarricense de Pesca (FECOP), and the associated academic institutions that made the Pacific Color 2025 campaign possible.
3. **Collaboration:** For projects utilizing unpublished or recently released data, early communication with the Chief Scientist and Principal

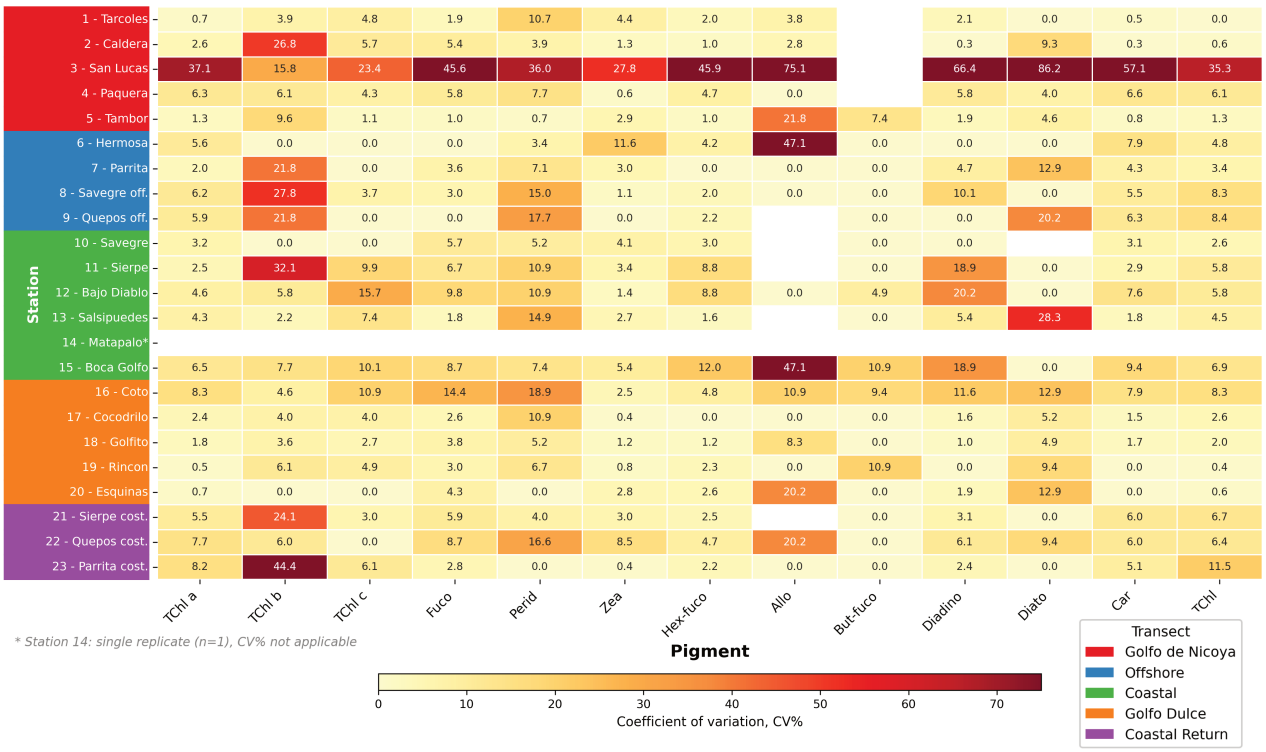


Figure A1. Replicate precision of HPLC-measured phytoplankton pigment concentrations across 23 stations sampled during the Pacific Color campaign (February 17–21, 2025) aboard the sportfishing yacht *Amejaye*. Precision is expressed as the coefficient of variation (CV%) computed from duplicate (or triplicate, **Stn. 21**) replicates. Annotated values reflect true CV%. **Stn. 14** (Matapalo) yielded a single valid replicate and CV% could not be calculated. **Stn. 3** (San Lucas) exhibited anomalously high CV% across most pigments due to physical degradation of one sample filter, as noted by the NASA GSFC HPLC facility. That observation has been removed from data analyses. NaN cells (white) for individual pigments at other stations indicate that one or both replicates were below the detection limit. Row colors denote sampling transect as indicated. Analysis performed by the NASA GSFC HPLC laboratory.

Investigators is highly encouraged to ensure accurate interpretation of the data and to foster potential collaborations.

A.2 HPLC Replicate Statistics

A.2.1 Analytical Precision

Replicate precision across all measured pigments, expressed as percent coefficient of variation (CV%), is summarized in Fig A1. Primary diagnostic pigments generally met the 8% validation threshold across most stations, with modest exceedances confined to stations with concentrations near detection limits. TChl *a* met the 5% threshold at 13 of 22 stations with valid replicates (CV% range: 0.47–8.21% excluding the **Stn. 3** outlier). **Stn. 14** (Matapalo) yielded a single valid replicate precluding CV% calculation.

Stn. 3 (San Lucas) was a clear outlier, with CV% values ranging from 36% (TChl *a*) to 86% (Diatoxanthin), attributed to physical degradation of one filter as noted by the NASA GSFC HPLC facility. The higher-value replicate (TChl *a*: 8.13 mg m^{-3}) was adopted for all analyses, per facility recommendation.